The Astrophysical Journal, 735:38 (20pp), 2011 July 1 doi:10.1088/0004-637X/735/1/38

CROSS-CORRELATIONS OF THE Lyα FOREST WITH WEAK-LENSING CONVERGENCE. ANALYTICAL ESTIMATES OF SIGNAL-TO-NOISE RATIO AND IMPLICATIONS FOR NEUTRINO MASS AND DARK ENERGY

Alberto Vallinotto[1], Matteo Viel[2,3], Sudeep Das[4,5], and David N. Spergel[4]
[1] Center for Particle Astrophysics, Fermi National Accelerator Laboratory, P.O. Box 500, Kirk Rd. & Pine St., Batavia, IL 60510-0500, USA; avalli@fnal.gov
[2] INAF-Osservatorio Astronomico di Trieste, Via G. B. Tiepolo 11, I-34131 Trieste, Italy
[3] INFN-National Institute for Nuclear Physics, Via Valerio 2, I-34127 Trieste, Italy; viel@oats.inaf.it
[4] Princeton University Observatory, Peyton Hall, Ivy Lane, Princeton, NJ 08544, USA; sudeep@astro.princeton.edu, dns@astro.princeton.edu
[5] Berkeley Center for Cosmological Physics, LBNL and Department of Physics, University of California, Berkeley, CA 94720, USA
Received 2010 January 11; accepted 2011 April 11; published 2011 June 14

ABSTRACT

We expect a detectable correlation between two seemingly unrelated quantities: the four-point function of the cosmic microwave background (CMB) and the amplitude of flux decrements in quasar (QSO) spectra. The amplitude of CMB convergence in a given direction measures the projected surface density of matter. Measurements of QSO flux decrements trace the small-scale distribution of gas along a given line of sight. While the cross-correlation between these two measurements is small for a single line of sight, upcoming large surveys should enable its detection. This paper presents analytical estimates for the signal-to-noise ratio (S/N) for measurements of the cross-correlation between the flux decrement and the convergence, $\langle \delta\mathcal{F}\kappa \rangle$, and for measurements of the cross-correlation between the variance in flux decrement and the convergence, $\langle (\delta\mathcal{F})^2\kappa \rangle$. For the ongoing BOSS (SDSS-III) and Planck surveys, we estimate an S/N of 30 and 9.6 for these two correlations. For the proposed BigBOSS and ACTPOL surveys, we estimate an S/N of 130 and 50, respectively. Since $\langle (\delta\mathcal{F})^2\kappa \rangle \propto \sigma_8^4$, the amplitude of these cross-correlations can potentially be used to measure the amplitude of σ_8 at $z \sim 2\%$–2.5% with BOSS and Planck and even better with future data sets. These measurements have the potential to test alternative theories for dark energy and to constrain the mass of the neutrino. The large potential signal estimated in our analytical calculations motivates tests with nonlinear hydrodynamic simulations and analyses of upcoming data sets.

Key words: cosmic background radiation – gravitational lensing: weak – intergalactic medium – large-scale structure of universe – neutrinos

Online-only material: color figures

1. INTRODUCTION

The confluence of high-resolution cosmic microwave background (CMB) experiments and large-scale spectroscopic surveys in the near future is expected to sharpen our view of the universe. Arcminute-scale CMB experiments such as Planck,[6] the Atacama Cosmology Telescope[7] (ACTPOL; Hincks et al. 2010), the South Pole Telescope[8] (Staniszewski et al. 2009), QUIET,[9] and PolarBeaR[10] will chart out the small-scale anisotropies in the CMB. This will shed new light on the primordial physics of inflation, as well as the astrophysics of the low-redshift universe through the signatures of the interactions of the CMB photons with large-scale structure. Spectroscopic surveys like BOSS (McDonald et al. 2005; Seljak et al. 2005) and BigBOSS (Schlegel et al. 2009b) will trace the large-scale structure of neutral gas, probing the distribution and dynamics of matter in the universe. While these two data sets will be rich on their own, they will also complement and constrain each other. An interesting avenue for using the two data sets would be to utilize the fact that the arcminute-scale secondary anisotropies in the CMB are signatures of the same large-scale structure that is traced by the spectroscopic surveys, and study them in cross-correlation with each other. In this paper, we present the analytic estimates for one such cross-correlation candidate—that between the gravitational lensing of the CMB and the flux fluctuations in the Lyα forest.

The gravitational lensing of the CMB, or CMB lensing in short, is caused by the deflection of the CMB photons by the large-scale structure potentials (for a review see Lewis & Challinor 2006). On large scales, *Wilkinson Microwave Anisotropy Probe* (*WMAP*) measurements imply that the primordial CMB is well described as an isotropic Gaussian random field (Komatsu et al. 2009). On small scales, lensing breaks this isotropy and introduces a specific form of non-Gaussianity. These properties of the lensed CMB sky can be used to construct estimators of the deflection field that lensed the CMB. Therefore, CMB lensing provides us with a way of reconstructing a line-of-sight (los) projected density field from zero redshift to the last scattering surface, with a broad geometrical weighting kernel that gets most of its contribution from the $z = 1$–4 range (Hu & Okamoto 2002; Hirata & Seljak 2003; Yoo & Zaldarriaga 2008). While CMB lensing is mainly sensitive to the geometry and large-scale projected density fluctuations, the Lyα forest, the absorption in quasar (QSO) spectra caused by intervening neutral hydrogen in the intergalactic medium (IGM), primarily traces the small-scale distribution of gas (and hence, also matter) along the line of sight.

A cross-correlation between these two effects gives us a unique way to study how small-scale fluctuations in the density field evolve on top of large scale overdensity and underdensity, and how gas traces the underlying dark matter. This signal is

[6] http://www.rssd.esa.int/index.php?project=planck
[7] http://www.physics.princeton.edu/act
[8] http://pole.uchicago.edu
[9] http://quiet.uchicago.edu
[10] http://bolo.berkeley.edu/polarbear

therefore a useful tool to test to what extent the fluctuations in the Lyα flux relate to the underlying dark matter. Once that relationship is understood, it can also become a powerful probe of the growth of structure on a wide range of scales. Since both massive neutrinos and dark energy alter the growth rate of structure at $z \sim 2$, these measurements can probe their effects. This new cross-correlation signal should also be compared with other existing cross-correlations between CMB and large-scale structure (LSS) that have already been observed and that are sensitive to different redshift regimes (Peiris & Spergel 2000; Giannantonio et al. 2008; Hirata et al. 2008; Croft et al. 2006; Xia et al. 2009).

In this work, we build an analytic framework based on simplifying assumptions to estimate the cross-correlation of the first two moments of the Lyα flux fluctuation with the weak-lensing convergence κ, obtained from CMB lensing reconstruction, measured along the same los. The finite resolution of the spectrogram limits the range of parallel k-modes probed by the absorption spectra, and the finite resolution of the CMB experiments limits the range of perpendicular k-modes probed by the convergence measurements. These two effects break the spherical symmetry of the k-space integration. However, we show that by resorting to a power series expansion it is still possible to obtain computationally efficient expressions for the evaluation of the signal.

We then investigate the detectability of the signal in upcoming CMB and LSS surveys, and the extent to which such a signal can be used as a probe of neutrino masses and early dark energy (EDE) scenarios. A highlight of our results is that the estimated cross-correlation signal seems to have significant sensitivity to the normalization of the matter power spectrum σ_8. Consistency with CMB measurements—linking power spectrum normalization and the sum of the neutrino masses—allows us to use this cross-correlation to put additional constraint on the latter.

The structure of the paper is as follows. In Section 2, we introduce the two physical observables, the Lyα flux and the CMB convergence (Section 2.1), the cross-correlation estimators (Section 2.2), and their variances (Section 2.3). Our main result is presented in Section 2.4 where the signal-to-noise ratios (S/Ns) are computed. Section 2.5 contains a spectral analysis of the observables that aims at finding the Lyα wavenumbers that contribute most to such a signal. We focus on two cosmologically relevant applications in Sections 3.1 and 3.2, for massive neutrinos and EDE models, respectively. We conclude with a discussion in Section 4.

2. ANALYTICAL RESULTS

2.1. Physical Observables

2.1.1. Fluctuations in the Lyα Flux

Using the *fluctuating Gunn–Peterson approximation* (Gunn & Peterson 1965), the transmitted flux $\mathcal{F}$ along a los $\hat{n}$ is related to the density fluctuations of the IGM $\delta_{\rm IGM}$ by

$$\mathcal{F}(\hat{n}, z) = \exp[-A(1 + \delta_{\rm IGM}(\hat{n}, z))^{\beta}], \quad (1)$$

where A and β are two functions relating the flux fluctuation to the dark matter overdensities. These two functions depend on the redshift considered: A is of order unity and is related to the mean flux level, baryon fraction, IGM temperature, cosmological parameters, and the photoionization rate of hydrogen. A good approximation for its redshift dependence is $A(z) \approx 0.0023\,(1+z)^{3.65}$ (see Kim et al. 2007). β on the other hand depends on to the so-called IGM temperature–density relation and in particular on the power-law index of this relation (e.g., Hui & Gnedin 1997; McDonald 2003) and should be less dependent on redshift (unless temperature fluctuations due, for example, to reionization play a role; see McQuinn et al. 2009). For the calculation of signal/noise in the paper, we neglect the evolution of A and β with redshift. While the value of the correlators considered will depend on A and β, their S/N will not.

On scales larger than about 1 h^{-1}Mpc (comoving), which is about the Jeans length at $z = 3$, the relative *fluctuations* in the Lyα flux $\delta\mathcal{F} \equiv (\mathcal{F} - \bar{\mathcal{F}})/\bar{\mathcal{F}}$ are proportional to the fluctuations in the IGM density field (Bi & Davidsen 1997; Croft et al. 1998, 2002; Viel et al. 2002; Saitta et al. 2008). We assume that the IGM traces the dark matter on large scales,

$$\delta\mathcal{F}(\hat{n}, \chi) \approx -A\beta\delta_{\rm IGM}(\hat{n}, \chi) \approx -A\beta\delta(\hat{n}, \chi). \quad (2)$$

The (variance of the) flux fluctuation in the redshift range covered by the Lyα spectrum is then proportional to (the variance of) the fluctuations in dark matter:

$$\delta\mathcal{F}^r(\hat{n}) = \int_{\chi_i}^{\chi_Q} d\chi\, \delta\mathcal{F}^r(\hat{n}, \chi) \approx \int_{\chi_i}^{\chi_Q} d\chi\, (-A\beta)^r\, \delta^r(\hat{n}, \chi), \quad (3)$$

where the range of comoving distances probed by the Lyα spectrum extends from χ_i to χ_Q. The $r = 1$ case corresponds to the fluctuations in the flux and the $r = 2$ case corresponds to their variance. We stress that the above approximation is valid in linear theory neglecting not only the nonlinearities produced by gravitational collapse but also those introduced by the definition of the flux and those produced by the thermal broadening and peculiar velocities. Note that while the assumption of "tracing" between gas and dark matter distribution above the Jeans length is expected in the standard linear perturbation theory (Eisenstein & Hu 1998), the one between the flux and matter has been verified a posteriori using semi-analytical methods (Bi & Davidsen 1997; Zaroubi et al. 2006) and numerical simulations (Gnedin & Hui 1998; Croft et al. 1998; Viel et al. 2006) that successfully reproduce most of the observed Lyα properties. Furthermore, non-gravitational processes such as temperature and/or ultraviolet fluctuations in the IGM should alter the Lyα forest flux power and correlations in a distinct way as compared to the gravitational instability process and to linear evolution (e.g., Fang & White 2004; Croft 2004; Slosar et al. 2009).

2.1.2. Cosmic Microwave Background Convergence Field

The effective weak-lensing convergence $\kappa(\hat{n})$ measured along an los in the direction $\hat{n}$ is proportional to the dark matter overdensity δ through

$$\kappa(\hat{n}, \chi_F) = \frac{3H_0^2\Omega_m}{2c^2} \int_0^{\chi_F} d\chi\, W_L(\chi, \chi_F) \frac{\delta(\hat{n}, \chi)}{a(\chi)}, \quad (4)$$

where the integral along the los extends up to a comoving distance χ_F and where $W_L(\chi, \chi_F) = \chi(\chi_F - \chi)/\chi_F$ is the lensing window function. In what follows we consider the cross-correlation of Lyα spectra with the convergence field measured from the CMB, as in Vallinotto et al. (2009), in which case χ_F is the comoving distance to the last scattering surface. Note however that it is straightforward to extend the present treatment to consider the cross-correlation of the Lyα flux fluctuations with

convergence maps constructed from other data sets, like optical galaxy surveys.

It is necessary to stress here that Equation (1) above depends on the density fluctuations in the IGM, which in principle are distinct from the ones in the dark matter, whereas κ depends on the dark matter overdensities δ. If the IGM and dark matter overdensity fields were completely independent, the cross-correlation between them would inevitably yield zero. If however the fluctuations in the IGM and in the dark matter are related to one another, then cross-correlating κ and $\delta\mathcal{F}$ will yield a non-zero result. The measurement of these cross-correlations tests whether the IGM is tracing the underlying dark matter field and quantifies the bias between flux and matter.

2.2. The Correlators

2.2.1. Physical Interpretation

The two correlators $\langle\delta\mathcal{F}\kappa\rangle$ and $\langle\delta\mathcal{F}^2\kappa\rangle$ have substantially different physical meaning: κ is proportional to the over(under)density integrated along the los and is dominated by long-wavelength modes with $k \sim 10^{-2}\,h\,\mathrm{Mpc}^{-1}$. Intuitively, κ therefore measures whether a specific los is probing an overall over(under)dense region. If the IGM traces the dark matter field, then by Equation (3) $\delta\mathcal{F}$ is expected to measure the dark matter overdensity along the same los extending over the redshift range Δz spanned by the QSO spectrum. This implies that

1. $\langle\delta\mathcal{F}\kappa\rangle$ quantifies whether and how much the overdensities traced by the Lyα flux contribute to the overall overdensity measured all the way to the last scattering surface. Because both κ and $\delta\mathcal{F}$ are proportional to δ, it is reasonable to expect that this correlator will be dominated by modes with wavelengths of the order of hundreds of comoving Mpc. As such, this correlator may be difficult to measure as it may be more sensitive to the calibration of the Lyα forest continuum.
2. $\langle\delta\mathcal{F}^2\kappa\rangle$ measures the relationship between long-wavelength modes in the density and the amplitude of the variance of the flux. The variance on small scales and the amplitude of fluctuations on large scales are not coupled in linear theory. However, in nonlinear gravitational theory regions of higher mean density have higher matter fluctuations. These lead to higher amplitude fluctuations in flux (Zaldarriaga et al. 2001). Since $\langle\delta\mathcal{F}^2\kappa\rangle$ is sensitive to this interplay between long- and short-wavelength modes, this correlator is much more sensitive than $\langle\delta\mathcal{F}\kappa\rangle$ to the structure growth rate. Furthermore, because $\delta\mathcal{F}^2$ is sensitive to short wavelengths, this signal is dominated by modes with shorter wavelengths than the ones dominating $\langle\delta\mathcal{F}\kappa\rangle$. As such, this signal should be less sensitive to the fitting of the continuum of the Lyα forest.

2.2.2. Tree-level Approximation

In what follows we focus on obtaining analytic expressions for the correlations between the (variance of the) flux fluctuations in the Lyα spectrum and the CMB convergence κ measured along the same los. From Equations (3) and (4) above, it is straightforward to obtain the general expression for the signal:

$$\langle\delta\mathcal{F}^r(\hat{n})\kappa(\hat{n})\rangle = \frac{3H_0^2\Omega_m}{2c^2}\int_0^{\chi_F} d\chi_c \frac{W_L(\chi_c,\chi_F)}{a(\chi_c)} \times \int_{\chi_i}^{\chi_Q} d\chi_q\,(-A\beta)^r\,\langle\delta^r(\hat{n},\chi_q)\,\delta(\hat{n},\chi_c)\rangle. \tag{5}$$

Since the QSOs used to measure the Lyα forest lie at $z > 2$, it is reasonable to expect that nonlinearities induced by gravitational collapse will not have a large impact on the final results. In the following, we therefore calculate the $r = 1$ and $r = 2$ correlators at *tree level* in cosmological perturbation theory. While beyond the scope of the current calculation, we could include the effects of nonlinearities induced by gravitational collapse by applying the *hyperextended perturbation theory* of Scoccimarro & Couchman (2001) to the terms in Equation (5).

At tree level in perturbation theory, the redshift dependence of the matter power spectrum factorizes into $P(k,\chi_c,\chi_q) = P_L(k)\,D(\chi_c)\,D(\chi_q)$, where $P_L(k)$ denotes the zero-redshift linear power spectrum and $D(\chi)$ the growth factor at comoving distance χ. Furthermore, the correlator appearing in the integrand of Equation (5) depends on the separation $\Delta\chi = \chi_q - \chi_c$ between the two points running on the los and in general it will be significantly non-zero only when $|\Delta\chi| \leqslant \Delta\chi_0 \approx 150\,h^{-1}$Mpc. Also, at tree level in perturbation theory these correlators carry $2r$ factors of D.[11] Using the approximation

$$D(\chi_c) = D(\chi_q - \Delta\chi) \approx D(\chi_q), \tag{6}$$

$$W_L(\chi_c,\chi_F) = W_L(\chi_q - \Delta\chi,\chi_F) \approx W_L(\chi_q,\chi_F), \tag{7}$$

$$a(\chi_c) = a(\chi_q - \Delta\chi) \approx a(\chi_q), \tag{8}$$

we can then write $\langle\delta^r(\hat{n},\chi_q)\,\delta(\hat{n},\chi_c)\rangle \approx \xi_r(\Delta\chi)D^{2r}(\chi_q)$ and trade the double integration (over χ_c and χ_q) for the product of two single integrations over $\Delta\chi$ and χ_q. Equation (5) factorizes into

$$\langle\delta\mathcal{F}^r\kappa\rangle \approx (-A\beta)^r\frac{3H_0^2\Omega_m}{2c^2}\int_{\chi_i}^{\chi_Q} d\chi_q\frac{W_L(\chi_q,\chi_F)}{a(\chi_q)}D^{2r}(\chi_q) \times \int_{-\Delta\chi_0}^{\Delta\chi_0} d\Delta\chi\;\xi_r(\Delta\chi). \tag{9}$$

This is the expression used to evaluate the signal. The determination of an expression for ξ_r and of an efficient way for evaluating it is the focus of the rest of the section.

2.2.3. Window Functions

The experiments that measure the convergence and the flux fluctuations have finite resolutions. We approximate the effective window functions of these experiments by analytically tractable Gaussian function.

These two window functions act differently: the finite resolution of the CMB convergence measurements limits the accessible range of modes perpendicular to the los, $\vec{k}_\perp$, and the finite resolution of the Lyα spectrum limits the range of accessible modes $k_\parallel$ parallel to the los. This separation of the modes into the ones parallel and perpendicular to the los is intrinsically dictated by the nature of the observables and it cannot be avoided once the finite resolution of the various observational campaigns is taken into account. Because of this symmetry, the calculation is most transparent in cylindrical coordinates: $\vec{k} = k_\parallel\hat{n} + \vec{k}_\perp$.

The high-k (short-wavelength) cutoff scales for the CMB and Lyα modes are denoted by k_C and k_L, respectively. Furthermore, we also add a low-k (long-wavelength) cutoff for the Lyα forest to take into account the fact that wavelengths longer than the

[11] Note in fact that even though in the $r = 2$ case it would be reasonable to expect three factors of D, the first non-zero contribution to the three-point function carries four factors of D because the Gaussian term vanishes exactly.

spectrum will appear in the spectrum itself as a background. We denote this low-k cutoff by k_l. After defining the auxiliary quantities

$$\bar{k}^2 \equiv \frac{k_L^2\, k_l^2}{k_L^2 + k_l^2}, \tag{10}$$

$$\hat{k}^2 \equiv \frac{k_L^2\, k_l^2}{2k_l^2 + k_L^2}, \tag{11}$$

the window functions acting on the Lyα and on the CMB modes, denoted, respectively, by W_α and W_κ, are defined through

$$W_\alpha(k_\parallel, k_L, k_l) \equiv [1 - e^{-(k_\parallel/k_l)^2}]e^{-(k_\parallel/k_L)^2} = e^{-(k_\parallel/k_L)^2} - e^{-(k_\parallel/\bar{k})^2}, \tag{12}$$

$$W_\kappa(\vec{k}_\perp, k_C) \equiv e^{(-\vec{k}_\perp^2/k_C^2)}, \tag{13}$$

where the direction dependence of the two window functions has been made explicit.

We determine the values of the cutoff scales as follows. For the Lyα forest, we consider the limitations imposed by the spectrograph, adopting the two cutoff scales k_L and k_l according to the observational specifications. In particular, for BOSS we assume $k_L = 1.9\ h\,\mathrm{Mpc}^{-1}$ and $k_l = 0.01\ h\,\mathrm{Mpc}^{-1}$. For the reconstruction of the CMB convergence map, we compute the minimum variance lensing reconstruction noise following Hu and Okamoto (Hu & Okamoto 2002). We then identify the multipole l_c, where the signal power spectrum equals the noise power spectrum for the reconstructed deflection field (for $l > l_c$ the noise is higher than the signal). Finally, we translate the angular cutoff l_c into a three-dimensional Fourier mode k_C at the relevant redshift to keep only modes with $k \leqslant k_C$ in the calculation. Note that if we had used the shape of the noise curve instead of this Gaussian cutoff, we would have effectively retained more Fourier modes, thereby increasing the signal. However, to keep the calculations simple and conservative we use the above Gaussian window. In what follows we will present results for convergence map reconstructions from the data sets of two CMB experiments: Planck and a hypothetical CMB polarization experiment based on a proposed new camera for the ACTPOL. For the former, we adopt the sensitivity values of the nine frequency channels from the Blue Book (Planck Collaboration 2006). For the latter, we assume a hypothetical polarization-based CMB experiment with a 3 arcmin beam and 800 detectors, each having a noise-equivalent-temperature (NET) of 300 μK-$\sqrt{s}$ over 8000 deg^2 with an integration time of 3×10^7 s. We further assume that both experiments will completely cover the 8000 deg^2 footprint of BOSS.

2.2.4. Auxiliary Functions

Because the calculation has cylindrical rather than spherical symmetry, the evaluation of the correlators of Equation (9) is more complicated, particularly for $r > 1$. As shown in the Appendix, it is possible to step around this complication and to obtain results that are computationally efficient with the adoption of a few auxiliary functions that allow the integrations in k-space to be carried out in two steps, first integrating on the modes perpendicular to the los and subsequently on the ones parallel to the los. The perturbative results for the correlators are expressed as combinations of the following auxiliary functions:

$$\tilde{H}_m(k_\parallel; k_C) \equiv \int_{|k_\parallel|}^\infty \frac{k\,dk}{2\pi}\,\frac{P_L(k)}{m!}\left(\frac{k^2 - k_\parallel^2}{k_C^2}\right)^m \exp\left(-\frac{k^2 - k_\parallel^2}{k_C^2}\right), \tag{14}$$

$$\tilde{L}_m(k_\parallel; k_C) \equiv \int_{|k_\parallel|}^\infty \frac{dk}{2\pi k}\,\frac{P_L(k)}{m!}\left(\frac{k^2 - k_\parallel^2}{k_C^2}\right)^m \exp\left(-\frac{k^2 - k_\parallel^2}{k_C^2}\right), \tag{15}$$

$$f_m^{(n)}(\Delta\chi; k_C, k_L) \equiv \int_{-\infty}^\infty \frac{dk_\parallel}{2\pi}\left(\frac{k_\parallel}{k_L}\right)^n \exp\left[-\frac{k_\parallel^2}{k_L^2} + ik_\parallel\Delta\chi\right] \times \tilde{f}_m(k_\parallel; k_C) \quad \text{with } f = \{L, H\}, \tag{16}$$

$$\bar{f}_0^{(n)}(s) \equiv \int_{-\infty}^\infty \frac{dk}{2\pi}\left(\frac{k}{s}\right)^n [e^{-2k^2/s^2} - e^{-k^2/\hat{k}^2}]\tilde{f}_0(k; \infty) \times \text{with} f = \{L, H\}. \tag{17}$$

Equations (14) and (15) above represent an intermediate step, where the integration on the modes perpendicular to the los is carried out. Equations (16) and (17) are then used to carry out the remaining integration over the modes that are parallel to the los.

The symmetry properties of the auxiliary functions are as follows. The functions $\tilde{f}_m$ are *real and even* in $k_\parallel$ regardless of the actual value of m. This in turn implies that $f_m^{(n)}$ are real and even (imaginary and odd) in $\Delta\chi$ when n is even (odd). Furthermore, the coefficients $\bar{f}_0^{(n)}$ are real and non-zero only if n is even, thus ensuring that $\xi_r(\Delta\chi)$ is always real-valued.

2.2.5. The $\langle\delta\mathcal{F}\kappa\rangle$ Correlator

In the $r = 1$ case, it is straightforward to identify $\xi_1(\Delta\chi)$ with a two-point correlation function measured along the los. However, the intrinsic geometry of the problem and the inclusion of the window functions leads us to evaluate this correlation function in a way that is different from the usual case, where the spherical symmetry in k-space can be exploited. In the present case, we have

$$\xi_1(\Delta\chi) = H_0^{(0)}(\Delta\chi; k_C, k_L) - H_0^{(0)}(\Delta\chi; k_C, \bar{k}). \tag{18}$$

It is then straightforward to plug Equation (18) into Equation (9) to obtain $\langle\delta\mathcal{F}(\hat{n})\kappa(\hat{n})\rangle$.[12] In Figure 1, we show the absolute value of the cross-correlation of the convergence κ of the CMB with the Lyα flux fluctuations $\delta\mathcal{F}$ observed for a quasar located at redshift z and whose spectrum spans a range of redshift Δz. The cosmological model used (and assumed throughout this work) is a flat ΛCDM universe with $\Omega_\mathrm{m} = 0.25$, $h = 0.72$, and $\sigma_8 = 0.84$ consistent with the WMAP-5 cosmology (Komatsu et al. 2009). The left and right panels show the results for the resolution of Planck and of the proposed ACTPOL experiment. We artificially set $A = \beta = 1$, effectively "turning off" the physics of IGM: this choice is not dictated by any physical argument but from the fact that it makes apparent the dynamics of structure formation.

[12] We checked that in the limit where $k_L \to \infty$, $k_C \to \infty$, and $k_l \to 0$ the usual two-point correlation function is recovered. Whereas one would naively expect that letting $k_L = k_C$ and $k_l = 0$ would lead to recover the usual two-point function calculated exploiting spherical symmetry in k-space with a cutoff scale equal to the common k_L, this is actually *not* the case. The reason for this is that the volume of k-space over which the integration is carried out is different for the two choices of coordinate systems. In particular, the spherical case always includes fewer modes than the cylindrical one. The two results therefore coincide *only* in the $k_L \to \infty$ limit.

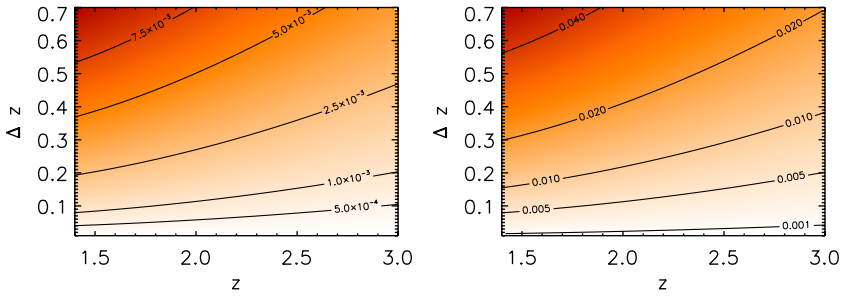

Figure 1. Absolute value of the correlator $\langle \delta \mathcal{F} \kappa \rangle$ along a *single* line of sight as a function of the source redshift z and of the length of the measured spectrum Δz, for convergence maps reconstructed from Planck (left panel, $k_C = 0.021\ h\,\mathrm{Mpc}^{-1}$) and ACTPOL (right panel, $k_C = 0.064\ h\,\mathrm{Mpc}^{-1}$). The value of the resolution of the QSO spectrum is the one predicted for SDSS-III, $k_L = 1.9\ h\,\mathrm{Mpc}^{-1}$. Also, we set $k_l = 0.01\ h\,\mathrm{Mpc}^{-1}$. To make the physics of structure formation apparent, we turn off the IGM physics by setting $A = \beta = 1$ (it is straightforward to rescale the values of the correlator to reflect different values of A and β).

(A color version of this figure is available in the online journal.)

The behavior of $\langle \delta \mathcal{F} \kappa \rangle$ shown in Figure 1 makes physical sense. Recall that this correlator is sensitive to the overdensity integrated along the redshift interval Δz (spanned by the QSO spectrum) that contributes to the CMB convergence. It then increases almost linearly with the length of the QSO spectrum Δz. It also increases if the resolution of the CMB experiment k_C is increased. An increased value of Δz corresponds to a longer Lyα spectrum, carrying a larger amount of information and thus leading to a larger correlation. Similarly, an increased value of k_C corresponds to a higher resolution of the reconstructed convergence map and therefore more modes—and information—being included in the correlation. Deepening the source's redshift (while keeping A and β fixed) on the other hand results in a *decrease* in $\langle \delta \mathcal{F} \kappa \rangle$. This fact is related to the growth of structure: the spectrum of a higher redshift QSO is probing regions where structure is less clumpy and therefore the absolute value of the correlation is smaller. Finally, once the redshift dependence of A is turned on (β is only mildly redshift dependent) the above result changes, leading to a final signal that is increasing with redshift.

We stress here that values of the correlators will be different when A and β are different from unity. Ultimately, these values should be recovered from a full nonlinear study based on large-scale high-resolution hydrodynamic simulations. However, numerical studies based on hydrodynamic simulations have shown convincingly that for both the flux power spectrum (two-point function) and flux bispectrum (three-point function) the shape is very similar to the matter power and bispectrum, while the amplitude is usually matched for values of A and β that are different from linear predictions (see the discussion in Viel et al. 2004). In this framework, nonlinear hydrodynamic simulations should at the end provide the "effective" values for A and β that will match the observed correlators and our results can be recasted in terms of these new parameters in a straightforward way.

2.2.6. The $\langle \delta \mathcal{F}^2 \kappa \rangle$ Correlator

The $r = 2$ case, where the variance of the flux fluctuation $\delta \mathcal{F}^2$ integrated along the los is cross-correlated with κ, is more involved. Looking back at Equations (5) and (9), it is possible to realize that the cumulant correlator $\langle \delta^2(\hat{n}, \chi_q)\, \delta(\hat{n}, \chi_c) \rangle = \xi_2(\Delta\chi)$ corresponds to a collapsed three-point correlation function, as two of the δ refer to the same physical point. The evaluation of ξ_2 is complicated by the introduction of the window functions W_α and W_κ. For the sake of clarity, we report here only the final results at tree level in cosmological perturbation theory, relegating the lengthy derivation to the Appendix. Letting

$$\xi_2(\Delta\chi) = \left\langle \delta_q^2 \delta_c \right\rangle_{1,2} + 2 \left\langle \delta_q^2 \delta_c \right\rangle_{2,3} \tag{19}$$

and using the auxiliary functions defined in Equations (14)–(17) above, it is possible to obtain the following series solution:

$$\begin{aligned}
\langle \delta^2 \delta \rangle_{1,2} = 2 \sum_{m=0}^{\infty} \Bigg\{ & \frac{5}{7} \Big[H_m^{(0)}(\Delta\chi, \chi_q; k_C, k_L) \\
& - H_m^{(0)}(\Delta\chi, \chi_q; k_C, \bar{k}) \Big]^2 \\
& + \Big[k_L\, H_m^{(1)}(\Delta\chi, \chi_q; k_C, k_L) - \bar{k}\, H_m^{(1)}(\Delta\chi, \chi_q; k_C, \bar{k}) \Big] \\
& \times \Big[k_L\, L_m^{(1)}(\Delta\chi, \chi_q; k_C, k_L) - \bar{k} L_m^{(1)}(\Delta\chi, \chi_q; k_C, \bar{k}) \Big] \\
& - m\, k_C^2 \Big[H_m^{(0)}(\Delta\chi, \chi_q; k_C, k_L) - H_m^{(0)}(\Delta\chi, \chi_q; k_C, \bar{k}) \Big] \\
& \times \Big[L_m^{(0)}(\Delta\chi, \chi_q; k_C, k_L) - L_m^{(0)}(\Delta\chi, \chi_q; k_C, \bar{k}) \Big] \\
& + \frac{2}{7} \Big[k_L^2\, L_m^{(2)}(\Delta\chi, \chi_q; k_C, k_L) - \bar{k}^2\, L_m^{(2)}(\Delta\chi, \chi_q; k_C, \bar{k}) \Big]^2 \\
& - \frac{4m}{7} k_C^2 \Big[k_L\, L_m^{(1)}(\Delta\chi, \chi_q; k_C, k_L) - \bar{k}\, L_m^{(1)}(\Delta\chi, \chi_q; k_C, \bar{k}) \Big]^2 \\
& + \frac{m(2m-1)}{7} k_C^4 \Big[L_m^{(0)}(\Delta\chi, \chi_q; k_C, k_L) \\
& - L_m^{(0)}(\Delta\chi, \chi_q; k_C, \bar{k}) \Big]^2 \Bigg\},
\end{aligned} \tag{20}$$

$$\begin{aligned}
\left\langle \delta_q^2 \delta_c \right\rangle_{2,3} = 2 \sum_{m=0}^{\infty} \frac{(-1)^m\, 2^m}{m!} \Bigg[& \frac{6}{7} \bar{H}_0^{(m)}(k_L) H_0^{(m)}(\Delta\chi; k_C, k_L) \\
& + \frac{1}{2} k_L^2 \bar{L}_0^{(m+1)}(k_L)\, H_0^{(m+1)}(\Delta\chi; k_C, k_L) \\
& + \frac{1}{2} k_L^2 \bar{H}_0^{(m+1)}(k_L)\, L_0^{(m+1)}(\Delta\chi; k_C, k_L) \\
& + \frac{3}{7} k_L^4\, \bar{L}_0^{(m+2)}(k_L)\, L_0^{(m+2)}(\Delta\chi; k_C, k_L) \\
& - \frac{k_L^2}{7} \bar{H}_0^{(m)}(k_L)\, L_0^{(m+2)}(\Delta\chi; k_C, k_L) \\
& - \frac{k_L^2}{7} \bar{L}_0^{(m+2)}(k_L)\, H_0^{(m)}(\Delta\chi; k_C, k_L) + (k_L \to \bar{k}) \Bigg].
\end{aligned} \tag{21}$$

In Figure 2, we show the result obtained using the tree-level expression for $\langle \delta \mathcal{F}^2 \kappa \rangle$, Equations (19)–(21). As before, we

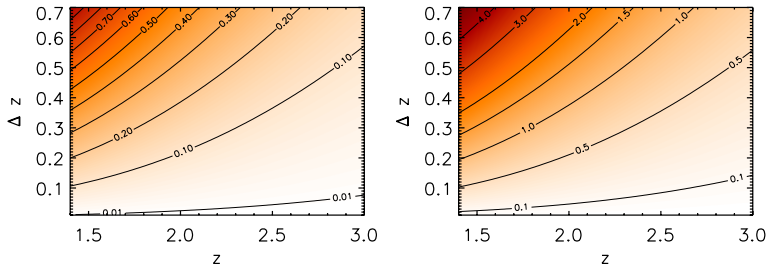

Figure 2. Absolute value of the correlator $\langle \delta\mathcal{F}^2\kappa\rangle$ along a *single* line of sight as a function of the source redshift z and of the length of the measured spectrum Δz, for convergence maps reconstructed from Planck (left panel, $k_C = 0.021\ h\,\mathrm{Mpc}^{-1}$) and ACTPOL (right panel, $k_C = 0.064\ h\,\mathrm{Mpc}^{-1}$). The value of the resolution of the QSO spectrum is the one predicted for SDSS-III, $k_L = 1.9\,h\,\mathrm{Mpc}^{-1}$. Also, we set $k_l = 0.01\,h\,\mathrm{Mpc}^{-1}$. As before, we set $A = \beta = 1$ to make the physics of structure formation apparent.

(A color version of this figure is available in the online journal.)

focus on the physics of structure formation and we turn off the IGM physics by setting $A = \beta = 1$. First, it is necessary to keep in mind that $\langle \delta\mathcal{F}^2\kappa\rangle$ is sensitive to the interplay of long- and short-wavelength modes and it probes the enhanced growth of short-wavelength overdensities that lie in an environment characterized by long-wavelength overdensities. The behavior of $\langle \delta\mathcal{F}^2\kappa\rangle$ with respect to z and Δz is similar to that of $\langle \delta\mathcal{F}\kappa\rangle$: it increases if Δz is increased or if the QSO redshift is decreased. However, the effect of the growth of structure is in this case stronger than in the previous case. This does not come as a surprise, as the growth of structure acts coherently in two ways on $\langle \delta\mathcal{F}^2\kappa\rangle$. Since in a ΛCDM model all modes grow at the same rate, a lower redshift for the source QSO implies larger overdensities on large scales which in turn enhance even further the growth of overdensities on small scales. Thus by lowering the source's redshift two factors play together to enhance the signal: first the fact that long- and short-wavelength modes have both grown independently, and second the fact that being coupled larger long-wavelength modes boost the growth of short-wavelength modes by a larger amount. This dependence is also made explicit in Equation (9), where we note that $\langle \delta\mathcal{F}^2\kappa\rangle$ depends on four powers of the growth factor. Finally, as before, the higher the resolution of the CMB experiment the larger is $d\langle \delta\mathcal{F}^2\kappa\rangle/d\Delta z$. This too makes physical sense, as a larger resolution leads to more modes contributing to the signal and therefore to a larger cross-correlation.

2.3. Variance of Correlators

To assess whether the correlations between fluctuations in the flux and convergence are detectable we need to estimate the S/N, which in turn requires the evaluation of the noise associated with the above observable. As mentioned above, both instrumental noise and cosmic variance are considered. We then move to estimate the variance of our correlator:

$$\sigma_r^2 \equiv \langle \delta\mathcal{F}^{2r}\kappa^2\rangle - \langle \delta\mathcal{F}^r\kappa\rangle^2. \tag{22}$$

Since $\langle \delta\mathcal{F}^r\kappa\rangle^2$ is just the square of the signal, we aim here to obtain *estimates* for $\langle \delta\mathcal{F}^{2r}\kappa^2\rangle$. From Equation (5), we get

$$\begin{aligned}\langle \delta\mathcal{F}^{2r}\kappa^2\rangle = &\left(A^r\beta^r\frac{3H_0^2\Omega_m}{2c^2}\right)^2\int_0^{\chi_F} d\chi_c\frac{W_L(\chi_c,\chi_F)}{a(\chi_c)}\\ &\times\int_0^{\chi_F} d\chi_c'\frac{W_L(\chi_c',\chi_F)}{a(\chi_c')}\int_{\chi_i}^{\chi_Q} d\chi_q\int_{\chi_i}^{\chi_Q} d\chi_q'\\ &\times\langle \delta^r(\hat{n},\chi_q)\,\delta^r(\hat{n},\chi_q')\,\delta(\hat{n},\chi_c)\delta(\hat{n},\chi_c')\rangle\,,\end{aligned} \tag{23}$$

where there are now two integrals running along the convergence los (on χ_c and χ_c') and two running along the Lyα spectrum (on χ_q and χ_q'). The correlator appearing in the integrand of Equation (23) is characterized by an even $(2r + 2)$ number of δ factors. This implies that an approximation to its value can be obtained using Wick's theorem. When Wick's theorem is applied, many different terms will in general appear. Adopting for the sake of brevity the notation $\delta(\hat{n},\chi_i') \equiv \delta_i$, terms characterized by the contraction of δ_i and δ_j will receive non-negligible contributions over the overlap of the respective los. The terms providing the largest contribution to $\langle \delta\mathcal{F}^{2r}\kappa^2\rangle$ are the ones where δ_c is contracted with $\delta_{c'}$: these terms in fact contain the value of the cosmic variance of the convergence and receive significant contributions from all points along the los from the observer all the way to the last scattering surface. On the other hand, whenever we consider the cross-correlation between a δ_c and a δ_q, this will acquire a non-negligible value only for those set of points where the los to the last scattering surface overlaps with the Lyα spectrum. As such, these terms are only proportional to the length of the Lyα spectrum, and thus sensibly smaller than the ones containing the variance of the convergence. We note in passing that the same argument should also apply to the connected part of the correlator, which should be significantly non-zero only along the Lyα spectrum. Mathematically, these facts become apparent from Equation (23) above, where terms containing $\langle \delta_c\delta_{c'}\rangle$ are the only ones for which the integration over χ_c and χ_c' can be traded for an integration over $\Delta\chi_c$ *and* an integration over χ_c that extends *all the way to* χ_F. If on the other hand δ_c is contracted with a δ_q factor, then the approximation scheme of Equations (6)–(8) leads to an integral over $\Delta\chi$ and to an integral over χ_q that extends only over the length probed by the Lyα spectrum. It seems therefore possible to safely neglect terms where the δ referring to the convergence are not contracted with each other.

2.3.1. The Variance of $\delta\mathcal{F}\kappa$

We start by considering the variance of $\delta\mathcal{F}\kappa$. Setting $r = 1$ in Equation (23) and using Wick's theorem, we obtain

$$\langle \delta_q\,\delta_{q'}\,\delta_c\,\delta_{c'}\rangle \approx 2\langle \delta_q\delta_c\rangle\langle \delta_{q'}\delta_{c'}\rangle + \langle \delta_q\delta_{q'}\rangle\langle \delta_c\delta_{c'}\rangle. \tag{24}$$

We note immediately that the first term is twice the square of $\langle \delta\mathcal{F}\kappa\rangle$, while the second term is proportional to two-correlation function characterized by cutoffs acting *either* on the modes that are parallel *or* perpendicular to the los, *but not on both*. It is then possible to show that

$$\begin{aligned}\langle \delta_q\delta_{q'}\rangle = D(\chi_q)\,D(\chi_{q'})\big[&H_0^{(0)}(\Delta\chi_q;\infty,\,k_L/\sqrt{2})\\ &- H_0^{(0)}(\Delta\chi_q;\infty,\,\bar{k}/\sqrt{2})\big],\end{aligned} \tag{25}$$

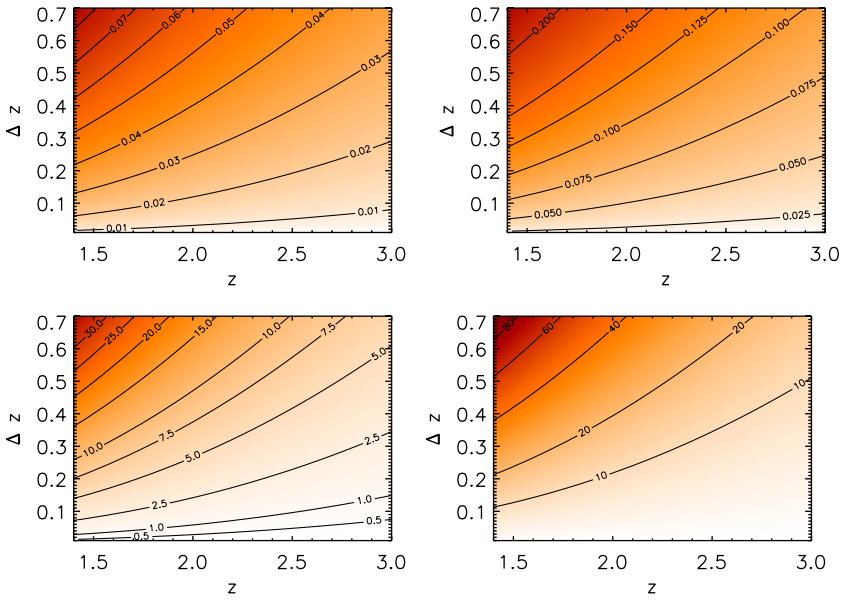

Figure 3. Estimates of the standard deviation of the correlator $\delta\mathcal{F}\kappa$ (upper panels) and $\delta\mathcal{F}^2\kappa$ (lower panels) along a *single* line of sight as a function of the source redshift z and of the length of the measured spectrum Δz, for convergence maps reconstructed from Planck (left panels) and ACTPOL (right panels). As before, we set $A = \beta = 1$, effectively turning off the physics of IGM, to make apparent the physics of structure formation.

(A color version of this figure is available in the online journal.)

$$\langle\delta_c\delta_{c'}\rangle = D(\chi_c)\,D(\chi_{c'})\,H_0^{(0)}(\Delta\chi_c; k_C/\sqrt{2}, \infty), \quad (26)$$

$$\langle\delta_q\delta_c\rangle = D(\chi_c)D(\chi_q) \times \left[H_0^0(\Delta\chi; k_C, k_L) - H_0^0(\Delta\chi; k_C, \bar{k})\right], \quad (27)$$

$$\langle\delta_q^2\rangle = D^2(\chi_q)\left[\bar{H}_0^{(0)}(\chi_q, k_L) + \bar{H}_0^{(0)}(\chi_q, \bar{k})\right], \quad (28)$$

where the last two equations have been added here for the sake of completeness, as they will be useful in what follows. The variance of $\delta\mathcal{F}\kappa$ is then

$$\sigma_1^2 \approx \langle\delta\mathcal{F}\,\kappa\rangle^2 + \left(A\beta\frac{3H_0^2\Omega_m}{2c^2}\right)^2 \times \int_0^{\chi_F} d\chi_c \frac{W_L^2(\chi_c, \chi_F)}{a^2(\chi_c)} D^2(\chi_c) \times \int_{\chi_i}^{\chi_Q} d\chi_q D^2(\chi_q) \int_{-\Delta\chi_{c,0}}^{\Delta\chi_{c,0}} d\Delta\chi_c H_0^{(0)}(\Delta\chi_c; k_C/\sqrt{2}, \infty) \times \int_{-\Delta\chi_{q,0}}^{\Delta\chi_{q,0}} d\Delta\chi_q\left[H_0^{(0)}(\Delta\chi_q; \infty, k_L/\sqrt{2}) - H_0^{(0)}(\Delta\chi_q; \infty, \bar{k}/\sqrt{2})\right]. \quad (29)$$

In the upper panels of Figure 3, we show the values obtained for the *standard deviation* of $\delta\mathcal{F}\kappa$ for two different CMB experiments' resolutions, again turning off the IGM physics evolution and focusing on the growth of structure.

2.3.2. The Variance of $\delta\mathcal{F}^2\kappa$

Setting $r = 2$ in Equation (23), we then apply Wick's theorem to $\langle\delta_q^2\delta_{q'}^2\delta_c\delta_{c'}\rangle$. Neglecting again terms where the δ_c are not contracted with one another, we obtain

$$\langle\delta_q^2\delta_{q'}^2\delta_c\delta_{c'}\rangle \approx 2\langle\delta_q^2\delta_c\rangle\langle\delta_{q'}^2\delta_{c'}\rangle + \langle\delta_c\delta_{c'}\rangle\left(\langle\delta_q^2\rangle\langle\delta_{q'}^2\rangle + 2\langle\delta_q\delta_{q'}\rangle^2\right), \quad (30)$$

which then leads to the expression for σ_2^2

$$\sigma_2^2 \approx \langle\delta\mathcal{F}^2\,\kappa\rangle^2 + \left(A\beta\frac{3H_0^2\Omega_m}{2c^2}\right)^2 \int_0^{\chi_F} d\chi_c \frac{W_L^2(\chi_c, \chi_F)}{a^2(\chi_c)} D^2(\chi_c) \times \int_{-\Delta\chi_{c,0}}^{\Delta\chi_{c,0}} d\Delta\chi_c H_0^{(0)}(\Delta\chi_c; k_C/\sqrt{2}, \infty) \times \left\{\left[\bar{H}_0^{(0)}(\chi_q, k_L) + \bar{H}_0^{(0)}(\chi_q, \bar{k})\right]^2\left[\int_{\chi_i}^{\chi_Q} d\chi_q D^2(\chi_q)\right]^2 + 2\int_{\chi_i}^{\chi_Q} d\chi_q D^4(\chi_q)\int_{-\Delta\chi_{q,0}}^{\Delta\chi_{q,0}} d\Delta\chi_q\left[H_0^{(0)}(\Delta\chi_q; \infty, k_L/\sqrt{2}) - H_0^{(0)}(\Delta\chi_q; \infty, \bar{k}/\sqrt{2})\right]^2\right\}. \quad (31)$$

In the lower panels of Figure 3, we show the estimates for the *standard deviation* $\delta\mathcal{F}^2\kappa$ along a *single* line of sight for the two different CMB experiments. We note in Figure 3 the same trends that have been pointed out for the correlator itself in Figures 1 and 2: the standard deviation of $\delta\mathcal{F}\kappa$ and of $\delta\mathcal{F}^2\kappa$ increases almost linearly with increasing length of the Lyα spectrum Δz and it decreases as the source redshift z is increased because of the fact that the spectrum probes regions that are less clumpy. Also, by increasing the resolution of the CMB experiment used to reconstruct the convergence map, the deviation of $\delta\mathcal{F}\kappa$ and $\delta\mathcal{F}^2\kappa$ also increases: if on the one hand more modes carry more information, on the other hand they also carry more cosmic variance.

One last aspect to note here is that while the signal for $\langle\delta\mathcal{F}^2\kappa\rangle$ arises from a three-point correlation function (which in the Gaussian approximation would yield zero), the dominant terms contributing to its variance arise from products of two-point correlation functions. In particular, it is possible to show

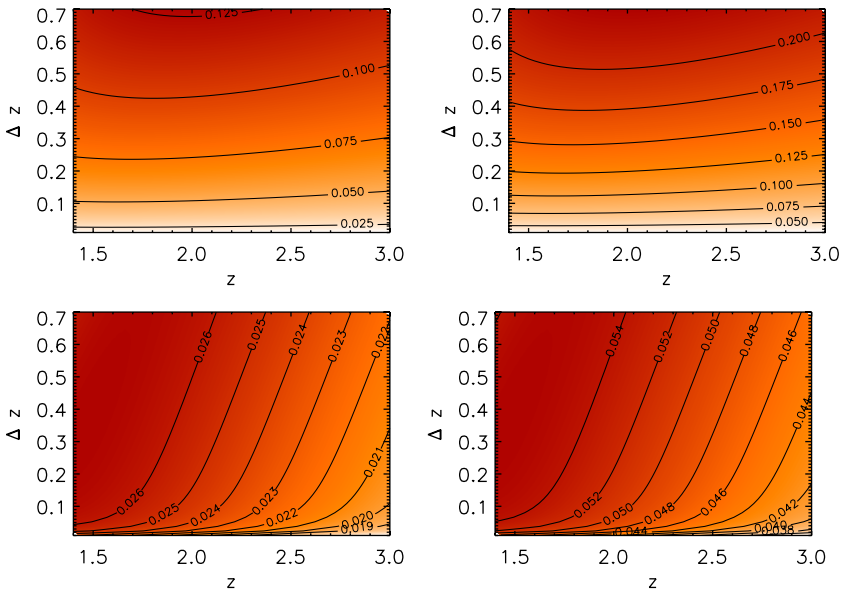

Figure 4. Estimates for the signal-to-noise ratios for the observation of the correlators $\langle \delta\mathcal{F}\kappa \rangle$ along a *single* line of sight as a function of the source redshift z and of the length of the measured spectrum Δz, for Planck (left panels) and ACTPOL (right panels). As long as the functions A and β can be assumed to be constant in the redshift range spanned by the Lyα spectrum, these results do not depend on the specific value taken by the latter.

(A color version of this figure is available in the online journal.)

that the terms appearing in the second line of Equation (30) significantly outweight the square of the signal that appears in the first line.

2.4. Signal-to-noise Ratio

We now have all the pieces to assess to what extent the $\langle \delta\mathcal{F}^r\kappa \rangle$ correlations will be detectable by future observational programs. Even before moving on to plot the S/Ns for $\delta\mathcal{F}\kappa$ and $\delta\mathcal{F}^2\kappa$ it is possible to point out a couple of features of these ratios. First, we note that the S/Ns for $\delta\mathcal{F}\kappa$ and $\delta\mathcal{F}^2\kappa$ do present a radical difference in their dependence on the QSO source redshift. This is because the signal for $\delta\mathcal{F}^2\kappa$ is characterized by mode coupling, whereas the dominant contributions to the variance are not. Physically, the signal for $\delta\mathcal{F}^2\kappa$ is more sensitive to the growth of structure with respect to its variance: while for the former the growth of long-wavelength modes enhances the growth of structure on small scales, for the latter long- and short-wavelength modes grow independently at the same rate. Mathematically, this is apparent when comparing Equation (9) with Equation (31): while the $\langle \delta\mathcal{F}^2\kappa \rangle$ signal carries four powers of the growth factor, the dominant terms contributing to its variance carry only six. In this case, the S/N then is characterized by four growth factors in the numerator and only three in the denominator, thus leading to a "linear" dependence of S/N on the redshift (modulo integration over the los and behavior of the lensing window function). Note that this is in stark contrast with the $\langle \delta\mathcal{F}\kappa \rangle$ case, where the signal is not characterized by mode coupling and the number of growth factors is equal for the signal and its standard deviation, thus leading to an S/N with no dependence on the source's redshift.

Second, we note that S/N does not depend on the value of any constant. In particular, regardless of their redshift dependence, the S/N will not depend on the functions A and β used to describe the IGM. This is of course very important since in such a way, at least in linear theory and using the FGPA at first order, the dependence on the physics of the IGM cancels out when computing the S/N.

In Figure 4, we show the estimates for the S/N per los of the $\langle \delta\mathcal{F}\kappa \rangle$ (upper panels) and $\langle \delta\mathcal{F}^2\kappa \rangle$ (lower panels) measurements. As expected, while the S/N for $\langle \delta\mathcal{F}\kappa \rangle$ does not show any strong redshift dependence, the S/N for $\langle \delta\mathcal{F}^2\kappa \rangle$ decreases linearly with increasing source redshift: the growth of structure is indeed playing a role and shows that QSOs lying at lower redshift will yield a larger S/N. Also, in both cases an increase in the resolution of the experiment measuring the convergence field translates to a larger S/N and to a larger derivative of the S/N with respect to Δz. This is not surprising, as it is reasonable to expect that a higher resolution convergence map will be carrying a larger amount of information about the density field.

All this suggests is that depending on what the correlator one is interested in measuring, different strategies should be pursued. In the case of $\langle \delta\mathcal{F}\kappa \rangle$ increasing the length of the spectra will provide a better S/N. In the case of $\langle \delta\mathcal{F}^2\kappa \rangle$, however, Figure 4 suggests that an increase in the number of quasars will be more effective in producing a large S/N, whereas an increase in the redshift range spanned by the spectrum will increase the S/N only marginally.

Having obtained the S/N per los, we can then estimate the total S/N that will be obtained by cross-correlating the BOSS sample (1.6×10^5 QSOs) and the proposed BigBOSS sample (Schlegel et al. 2009b; 10^6 QSOs) with the convergence map measured by Planck or by the proposed ACTPOL experiment considered. Assuming a mean QSO redshift of $\bar{z} = 2.5$ and a mean Lyα spectrum length of $\Delta z = 0.5$, a rough estimate of the S/N for the measurements of $\langle \delta\mathcal{F}\kappa \rangle$ and of $\langle \delta\mathcal{F}^2\kappa \rangle$ is given in Tables 1 and 2.

It is necessary to point out here that despite the value of the S/N for $\langle \delta\mathcal{F}\kappa \rangle$ being almost three times larger than the one for $\langle \delta\mathcal{F}^2\kappa \rangle$, the actual measurement of the former correlator strongly depends on the ability of fitting the continuum of the Lyα spectrum. The $\langle \delta\mathcal{F}^2\kappa \rangle$ correlator, on the other hand, is sensitive to the interplay between long- and short-wavelength modes and as such should be less sensitive to the continuum fitting procedure. Therefore, even if it is characterized by a

Table 1
Estimates of the Total and Per Single los S/N of the $\langle \delta \mathcal{F} \kappa \rangle$ Cross-correlation for Different CMB Experiments Combined with BOSS and BigBOSS

CMB Exp.	S/N per los	Total S/N in BOSS	Total S/N in BigBOSS
Planck	0.075	30	75
ACTPOL	0.130	52	130

Table 2
Estimates of the Total and Per Single los S/N of the $\langle \delta \mathcal{F}^2 \kappa \rangle$ Cross-correlation for Different CMB Experiments Combined with BOSS and BigBOSS

CMB Exp.	S/N per los	Total S/N in BOSS	Total S/N in BigBOSS
Planck	0.024	9.6	24
ACTPOL	0.05	20.0	50

lower S/N, it may actually be the easier to measure in practice. The numbers obtained above are particularly encouraging since the S/N values are typically very large and well above unity.

2.5. Analysis

Having developed a calculation framework for estimating $\langle \delta \mathcal{F}^r \kappa \rangle$ and the S/N for their measurement, we turn to estimating the range of Lyα wavelengths contributing to the signal and the effect of changing the parameters that control the experiments' resolution.

2.5.1. Spectral Analysis

We investigate here how the different Lyα modes contribute to the correlators. This should tell us whether long-wavelength modes have any appreciable effect on our observables and what the impact of short and very short wavelength modes is (in particular the ones that are expected to have entered the nonlinear regime).

Since the mean flux $\bar{\mathcal{F}}$ appearing in the definition of the flux fluctuation $\delta \mathcal{F} = (\mathcal{F} - \bar{\mathcal{F}})/\bar{\mathcal{F}}$ is a *global* quantity which is usually estimated from a statistically significant sample of high-resolution QSO spectra (see the discussion in Seljak et al. 2003 for the impact that such a quantity has on some derived cosmological parameters), $\delta \mathcal{F}$ is also sensitive to modes with wavelengths longer than the Lyα spectrum. These modes appear as a "background" in each spectra but they still have to be accounted for when cross-correlating $\delta \mathcal{F}$ with κ because the fluctuation in the flux is affected by them. More specifically, a QSO that is sitting in an overdense region that extends beyond the redshift range spanned by its spectrum will see its flux decremented by a factor that in its spectrum will appear as a *constant* decrement. On the other hand, if the QSO spectrum extends beyond the edge of such overdensity, this mode would appear as a fluctuation (and not as a background) in the spectrum. This extreme scenario is somewhat mitigated by the fact that present and future QSO surveys will have many QSOs with los separated by a few comoving Mpc (Schlegel et al. 2009a): as such, fluxes from neighboring QSOs lying in large overdense regions should present similarities that should in principle allow to detect such large overdensities in three-dimensional tomographical studies (Saitta et al. 2008).

To measure the contributions of the different modes to the correlators, we vary k_l and k_L to build appropriate filters. As can be seen from Figure 5, where three such filters are plotted for $\{k_l = 0.001, k_L = 0.01\}$, $\{k_l = 0.01, k_L = 0.1\}$, and $\{k_l = 0.1, k_L = 1\}$, the Gaussian functional form assumed for the window function does not provide very sharp filters (hence this spectral analysis will not reach high resolution). Also, if $k_L = 10\, k_l$ then the filters add exactly to one. This allows us to measure the contributions of the different wavenumber decades to the correlators and its standard deviation.

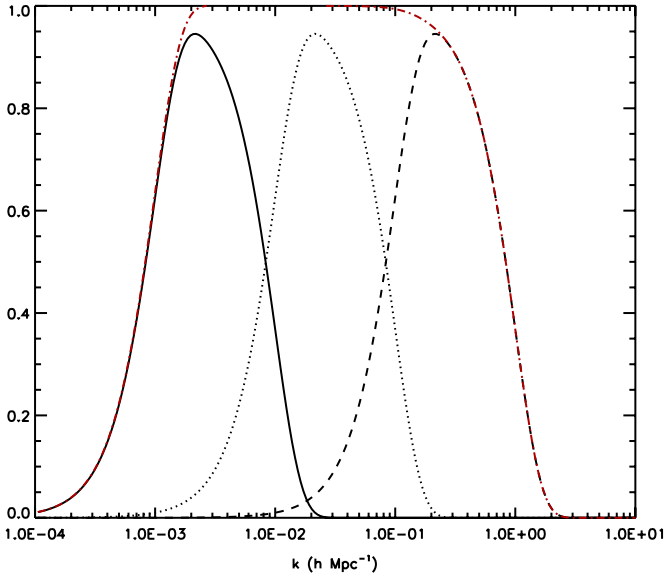

Figure 5. Three filters used to calculate the contribution of the different modes to the correlators, their variance, and the SN ratio. The filters have $\{k_l = 10^{-3}, k_L = 10^{-2}\}$ (solid curve), $\{k_l = 10^{-2}, k_L = 10^{-1}\}$ (dotted curve), and $\{k_l = 10^{-1}, k_L = 1\}$ (dashed curve). Also shown is the sum of the filters (red dash-dotted curve).

(A color version of this figure is available in the online journal.)

Table 3
Contribution of the Different Wavenumbers (Split over Decades) to the Absolute Value of the Correlator $\langle \delta \mathcal{F} \kappa \rangle$, Its Standard Deviation $\sigma_{\delta \mathcal{F} \kappa}$, and Ratio of the Two Quantities

k_l	k_L	$\lvert\langle \delta \mathcal{F} \kappa \rangle\rvert$	$\sigma_{\delta \mathcal{F} \kappa}$	Ratio
1.00e−04	1.00e−03	1.66e−04	1.77e−04	9.39e−01
1.00e−03	1.00e−02	1.20e−03	1.21e−03	9.87e−01
1.00e−02	1.00e−01	2.12e−04	6.29e−04	3.37e−01
1.00e−01	1.00e+00	6.11e−07	1.42e−03	4.30e−04
1.00e+00	1.00e+01	7.26e−08	2.44e−03	2.97e−06

Note. In this calculation, we took into account the evolution of A with redshift.

Table 4
Contribution of the Different Wavenumbers (Split over Decades) to the Correlator $\langle \delta \mathcal{F}^2 \kappa \rangle$, Its Standard Deviation $\sigma_{\delta \mathcal{F}^2 \kappa}$, and Ratio of the Two Quantities

k_l	k_L	$\langle \delta \mathcal{F}^2 \kappa \rangle$	$\sigma_{\delta \mathcal{F}^2 \kappa}$	Ratio
1.00e−04	1.00e−03	1.08e−04	2.18e−02	4.99e−03
1.00e−03	1.00e−02	6.69e−03	1.96e−01	3.40e−02
1.00e−02	1.00e−01	5.92e−02	1.31e+00	4.52e−02
1.00e−01	1.00e+00	3.39e−01	7.06e+00	4.80e−02
1.00e+00	1.00e+01	9.92e−01	2.07e+01	4.79e−02

Note. In this calculation, we took into account the evolution of A with redshift.

Tables 3 and 4 summarize the results for $\langle \delta \mathcal{F} \kappa \rangle$ and $\langle \delta \mathcal{F}^2 \kappa \rangle$, respectively. Considering $\langle \delta \mathcal{F} \kappa \rangle$ we note immediately that the signal and the S/N both peak around $k \simeq 10^{-2}\ h\,\mathrm{Mpc}^{-1}$, as expected from the fact that this signal is proportional to

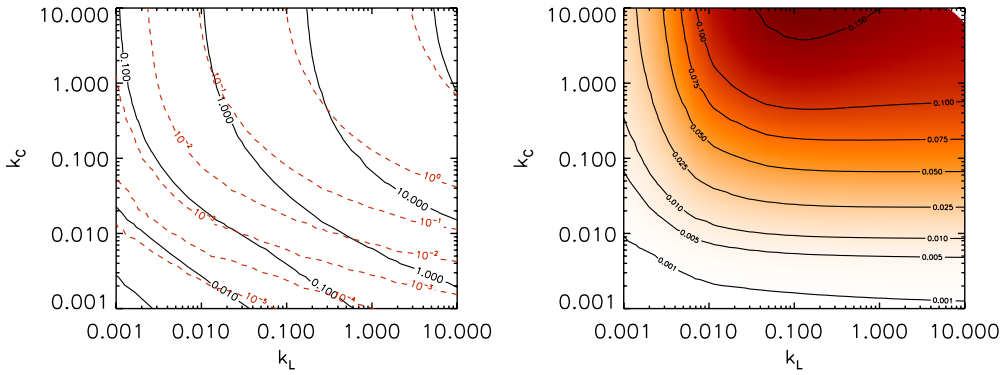

Figure 6. Value of $\langle \delta \mathcal{F}^2 \kappa \rangle$ (left panel, red dashed contours), its standard deviation (left panel, black solid contour), and its S/N (right) for a single QSO lying at $z = 2.6$ and whose spectrum covers $\Delta z = 0.5$. Here we assume $k_l = 0$ and $A = \beta = 1$.

(A color version of this figure is available in the online journal.)

the two-point correlation function, which in turn receives its largest contribution from the wavelengths that dominate the power spectrum: isolating the long-wavelength modes of the Lyα flux would allow to increase the S/N. However, this procedure is sensibly complicated by the continuum fitting procedures that are needed to correctly reproduce the long-wavelength fluctuations of the Lyα flux. The behavior of the variance is interesting, as in the first three decades it shows an oscillating behavior. This is due to the different weights of the two terms appearing in Equation (29) for each range of wavelengths. In particular, for $k \lesssim 10^{-2}\ h\,\mathrm{Mpc}^{-1}$ the variance of $\langle \delta \mathcal{F} \kappa \rangle$ is dominated by the first term that is just the square of the signal. However, as the signal gets smaller with increasing k, for $k \gtrsim 10^{-1}\ h\,\mathrm{Mpc}^{-1}$ it is the second term that dominates the variance.

Regarding $\langle \delta \mathcal{F}^2 \kappa \rangle$, it is necessary to point out two aspects. First, short-wavelength (high-k) modes provide the larger contribution to *both* the correlator *and* its standard deviation. Second, for $k \gtrsim 10^{-2}\ h\,\mathrm{Mpc}^{-1}$ the ratio of the contribution to the correlator and to its standard deviation remains almost constant. This means that above $10^{-2}\ h\,\mathrm{Mpc}^{-1}$ the different frequency ranges contribute roughly in the same proportion. This fact is both good news and bad news at the same time. It is bad news because it means that increasing the resolution of the Lyα spectra does not automatically translate into increasing the *precision* with which the correlator will be measured, as the high-k modes that are introduced will boost both the correlator and its variance in the same way. On the other hand, this appears to be good news because it tells us that low-resolution spectra which do not record nonlinearities on small scales can be successfully used to measure this correlation. To increase the S/N and to achieve a better precision for this measurement, it is better to increase the number of QSO spectra than to increase the resolution of each single spectra. Finally, cutting off the long-wavelength modes with $k \lesssim 10^{-2}\ h\,\mathrm{Mpc}^{-1}$ should *not* have a great impact on the S/N or on the measured value of the correlator: if on the one hand the contribution of the modes with $k \lesssim 10^{-2}\ h\,\mathrm{Mpc}^{-1}$ is noisier due to cosmic variance, on the other hand the absolute value of such contributions to the correlator and to its variance is negligible compared to the ones arising from $k \gtrsim 10^{-2}\ h\,\mathrm{Mpc}^{-1}$. We can see this fact also comparing the last column of Table 4 with the right panel of Figure 6 where the *absolute value* of the S/N is plotted for varying values of the cutoffs k_L and k_C. Looking at the last column of Table 4, we see that the ratio between the correlator and its standard deviation increases until about $k \simeq 10^{-2}\ h\,\mathrm{Mpc}^{-1}$ where it levels off. Looking at the right panel of Figure 6, we note exactly the same trend: increasing the resolution of the spectrum k_L above $10^{-2}\ h\,\mathrm{Mpc}^{-1}$ does not improve dramatically the S/N. This is because from that point on each new mode contributes in almost the same amount to the correlator and to its standard deviation.

2.5.2. Dependence on Experimental Resolutions

To analyze the impact of a change in the resolution of the experiments measuring the CMB convergence map or the Lyα flux, we consider a single QSO at redshift $z_0 = 2.6$, whose spectrum covers $\Delta z = 0.5$, and vary k_L and k_C. In this case we set $k_l = 0$.

In Figure 6, we show the value of $\langle \delta \mathcal{F}^2 \kappa \rangle$, its standard deviation, and its S/N for varying values of k_L and k_C. We note that both the correlator and its standard deviation increase with increasing resolution: this makes physical sense as increasing the resolution increases both the amount of information carried by each experiment and the cosmic variance associated with it. Except for very low values of k_C, an increase in the resolution of the Lyα spectrum is characterized by an almost equal amount of increase in both the correlator and its cosmic variance. This implies that the S/N becomes roughly constant for $k_L \gtrsim 10^{-2}\ h\,\mathrm{Mpc}^{-1}$. On the other hand, increasing k_C increases both the correlator and its cosmic variance only up to the point where $k_C \simeq k_L$.

2.6. Comparison with Numerical Simulations

This work aims at presenting *analytical* estimates for the value of $\langle \delta \mathcal{F} \kappa \rangle$ and $\langle \delta \mathcal{F}^2 \kappa \rangle$ and their detectability as a function of the experiments' resolutions and cosmological parameters. A detailed analysis of the correlators using results from numerical simulations goes beyond the scope of the present work and is the aim of a forthcoming publication. We pause here, however, to briefly report on a few preliminary results obtained using numerical simulations. In particular, we address the impact of redshift space distortions and instrumental noise using mock QSO spectra on simulated quantities. To this end, we extract 1000 lines of sight from a cosmological simulation which consists of a periodic volume of linear size $512\ h^{-1}$ comoving Mpc with 2×512^3 gas and dark matter particles. The cosmological parameters are in rough agreement with recent estimates from large-scale structure data: $\Omega_{0m} = 0.3$, $\Omega_{0\Lambda} = 0.7$, $\Omega_{0b} = 0.05$, $n_s = 0.95$, and $H_0 = 70\ \mathrm{km\ s^{-1}\ Mpc^{-1}}$. The code used is the parallel TREE–smoothed particle hydrodynamic code GADGET-II (Springel 2005). This simulation cannot resolve

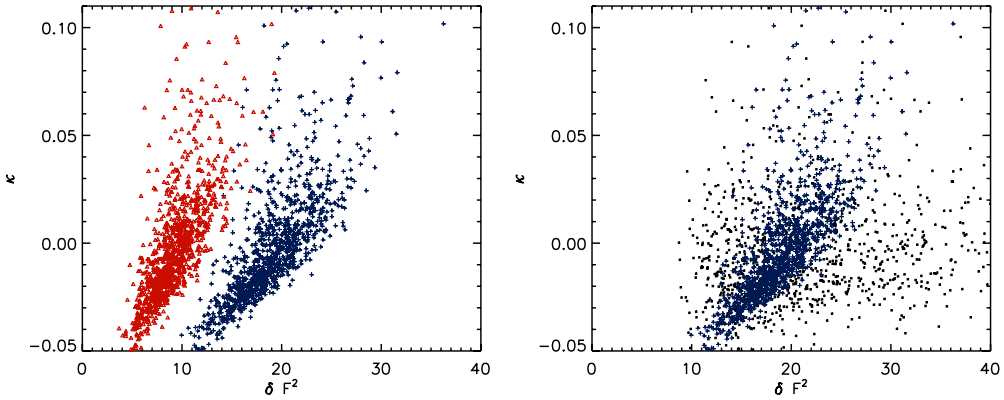

Figure 7. Scatter plot of κ measured along the QSO spectrum and $\delta\mathcal{F}^2$ for 1000 QSOs at $z = 2$. In the left panel, we compare spectra with (blue crosses) and without (red triangles) redshift space distortions. In the right panel, we compare the same spectra with redshift space distortions (blue crosses) with the same one obtained taking into account BOSS instrumental resolution and noise (black squares).

(A color version of this figure is available in the online journal.)

the Jeans length (the gravitational softening is chosen to be 33 kpc h^{-1}) but should at least allow us to accurately reproduce the properties of the flux at large scales and to be quantitatively better than the fluctuating Gunn–Peterson approximation by including several nonlinear effects. The procedure of extracting mock QSO spectra can also be performed by switching on and off the peculiar velocity and resolution and adding noise to the spectra in order to roughly mimic the Sloan Digital Sky Survey (SDSS) spectra: resolution $\sim$70 km s^{-1}, pixel size $\sim$70 km s^{-1}, and S/N equal to five.

For each one of these los's, we evaluate $\delta\mathcal{F}$, $\delta\mathcal{F}^2$, and the contribution of κ along the quasar los, carrying out the integral of Equation (4) *only* over the range of comoving distances covered by the spectrum. Since the variance of $\langle\delta\mathcal{F}^2\kappa\rangle$ is dominated by the terms proportional to $\langle\kappa^2\rangle$, measuring $\langle\delta\mathcal{F}\kappa\rangle$ and $\langle\delta\mathcal{F}^2\kappa\rangle$ using these values of κ would be incorrect. However, the point we want to address here is the impact of peculiar velocities and instrumental noise and to this end a different value of the dispersion of κ will not alter the conclusions we are going to draw on these effects.

2.6.1. Impact of Redshift Space Distortions

To assess the impact of peculiar velocities, we show in Figure 7 (left panel) a scatter plot for two sets of points. Both sets are obtained using 1000 QSO spectra for quasar located at $z = 2$, but while the first set (red points) is obtained neglecting redshift space distortions, the second one (blue points) is obtained taking the latter into account. As can be seen from Figure 7, redshift space distortions do not significantly alter the correlation. In particular, both a Bayesian and a non-parametric analysis of these data show that this correlation remains statistically significant when redshift space distortions are included in the picture.

2.6.2. Impact of Instrumental Noise

To assess the impact of instrumental noise in the measurement of QSO spectra, we degrade the synthetic spectra to match BOSS resolution. Next, we add instrumental noise. In Figure 7 (right panel), we show the scatter plot of $\delta\mathcal{F}^2$ versus κ. Again, we show two sets of points. The first set (blue points) is the one considered above, which includes the redshift space distortions. The second set (black points) is the set obtained including instrumental resolution and noise. It is clear that low spectra resolution and instrumental noise sensibly degrade the correlation. However, carrying out a Spearman non-parametric rank correlation test, the correlation between $\delta\mathcal{F}^2$ and κ is still statistically significant at more than 99% confidence level (CL). We have therefore reason to suggest that with the large number of los's available in BOSS, this correlation will remain detectable even when the full value of κ from the observer all the way to the last scattering surface is taken into account.

3. COSMOLOGICAL APPLICATIONS

3.1. Neutrinos

Massive neutrinos are known to suppress the growth of structure in the early universe on intermediate-to-small scales, $k \gtrsim 10^{-2}\ h\,\mathrm{Mpc}^{-1}$ (Lesgourgues & Pastor 2006). Since $\langle\delta\mathcal{F}^2\kappa\rangle$ is mostly sensitive to the same range of scales, it seems reasonable to examine to what extent massive neutrinos will alter the $\langle\delta\mathcal{F}^2\kappa\rangle$ signal. The argument could also be turned around, asking how well a measurement of $\langle\delta\mathcal{F}^2\kappa\rangle$ would allow us to constrain the sum of the neutrino masses. In this first work, we take the first route and simply calculate how the $\langle\delta\mathcal{F}^2\kappa\rangle$ signal is affected by different values of the neutrino masses. We leave the analysis of the constraining power of $\langle\delta\mathcal{F}^2\kappa\rangle$ to a forthcoming work.

Quite generally massive neutrinos affect the matter density power spectrum in a scale-dependent way (see Lesgourgues & Pastor 2006 for a review). To account for this effect in an exact way would require substantial modifications of the formalism and of the code that we are currently using to evaluate $\langle\delta\mathcal{F}^2\kappa\rangle$. In particular, it would no longer be possible to separate the integrations over the comoving distance from the ones over the wavenumbers k. We leave this important development to a future project and for the purpose of this work we rely on the following approximation (Hu & Eisenstein 1998) for the growth of the dark matter perturbations:

$$\delta_{\mathrm{cdm}} \propto D(a)^{1-\frac{3}{5}f_\nu}, \tag{32}$$

where $f_\nu \equiv \Omega_\nu/\Omega_m$. The above expression is accurate at very large scales down to the largest scales probed by the Lyα forest, while departures at smaller scales are best handled with N-body or hydrodynamic codes that properly model the nonlinear evolution (Brandbyge et al. 2008; Viel et al. 2010).

The second aspect that we need to take into account before proceeding with the calculation is that consistency with CMB

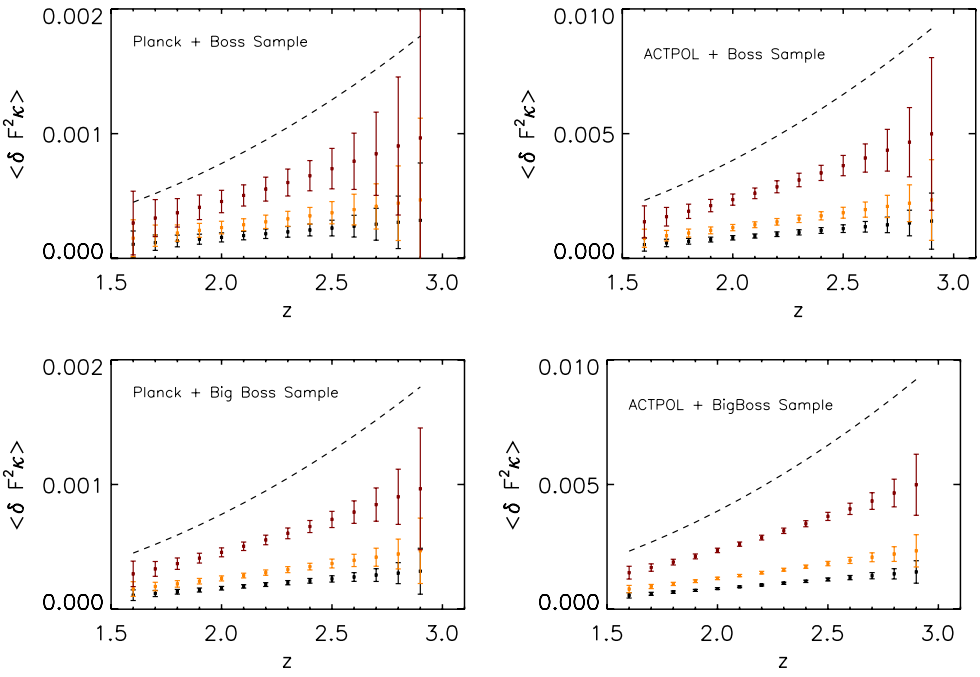

Figure 8. Cross-correlation of the variance of the Lyα flux and CMB convergence as a function of redshift for the three different cosmological models with massive neutrinos shown in Table 4. Black, orange, and red (with 1σ) error bars refer to $\Sigma m_\nu(\mathrm{eV}) = 0.54, 0.4, 0.15$, respectively. The black dashed line shows the prediction for a massless neutrino cosmology consistent with WMAP-5 data. Four different cases are reported here for Planck+BOSS (top left), Planck + BigBOSS (bottom left), ACTPOL+BOSS (top right), and ACTPOL+BigBOSS (bottom right). The redshift evolution of A is taken into account here.

(A color version of this figure is available in the online journal.)

Table 5
Values of the Cosmological Parameters Assumed to Estimate the Effect of Massive Neutrinos on $\langle\delta\mathcal{F}^2\kappa\rangle$

Num.	Ω_m	Ω_Λ	Ω_ν	Σm_ν(eV)	σ_8	h
1	0.269	0.719	1.2e−2	0.54	0.657	0.70
2	0.269	0.722	8.8e−3	0.40	0.708	0.70
3	0.269	0.728	3.3e−3	0.15	0.786	0.70
4	0.256	0.744	0.0	0.0	0.841	0.72

Note. All models assume flat geometry.

data requires that a change in the sum of the neutrino masses is accompanied by a change in the power spectrum normalization σ_8 (Komatsu et al. 2009). This fact has a profound consequence. Just by counting the number of powers of the power spectrum that enter in the different expressions, it is straightforward to note that $\langle\delta\mathcal{F}^2\kappa\rangle \sim \sigma_8^4$, that $\sigma^2_{\langle\delta\mathcal{F}^2\kappa\rangle} \sim \sigma_8^6$, and that its S/N is proportional to σ_8.[13] Consequently, a change in the neutrino masses, which requires a change in σ_8 to maintain consistency with CMB data, will cause a change in $\langle\delta\mathcal{F}^2\kappa\rangle$.

To take this into account, we proceed as follows. First, we consider the set of values allowed by the WMAP-5 data in the $\sigma_8 - \Sigma m_\nu$ space at 95% CL. These correspond to the dark red area of the center panel of Figure 17 in Komatsu et al. (2009). We then choose three flat models with massive neutrinos consistent with the WMAP-5 data and use CAMB to generate the respective dark matter power spectra to be used in the calculation. The value of the cosmological parameters used for each model is summarized in Table 5.

One last point is left to be considered. Note in fact that the S/N for $\langle\delta\mathcal{F}^2\kappa\rangle$, although increasing with Δz, does not increase at a very high rate. It seems therefore possible to speculate that subdividing the Lyα spectra into sub-spectra, each of length $dz = 0.1$, despite lowering the S/N for each single sub-spectrum, would allow us to reach a better measurement of the redshift dependence of the signal.

Figure 8 below shows the result of applying the latter procedure. The black, orange, and red data points represent predicted values of the $\langle\delta\mathcal{F}^2\kappa\rangle$ correlator for values of $\sum m_\nu = \{0.54, 0.4, 0.15\}$, respectively, while the dashed black line shows the value of the correlator for a ΛCDM cosmology with massless neutrinos. As one can see, the cross-correlation signal is quite sensitive to the presence of massive neutrinos and already BOSS and Planck could provide constraints on the strength of such correlators. As pointed out above, this is due to the fact that more massive neutrinos require smaller values of σ_8, which in turn depresses the signal.

It is here necessary to point out one important caveat. In this paper, we are making a tree-level approximation to the growth rate of k modes: this enables us to separate integrations along the comoving distances from integrations on the different modes. As previously mentioned, this approximation does not include the scale-dependent effects of neutrinos on the growth rate of structure. Similarly, this approximation also does not allow us to take into account the nonlinearities induced by gravitational collapse, which on the other hand tend to enhance the power spectrum on small scales. We will need to either use hyperextended perturbation theory results or nonlinear simulations to evaluate these effects.

3.2. Early Dark Energy

Since EDE or deviations from general relativity affect the growth rate of structure as a function of scale, the measurements of $\langle\delta\mathcal{F}^2\kappa\rangle(z)$ can in principle probe these effects. Here we focus on EDE models, where dark energy makes a significant

[13] We warn however that these scalings are valid only in the linear regime. More sophisticated nonlinear modeling and numerical simulations are needed in order to quantify more precisely the exact form of such scalings.

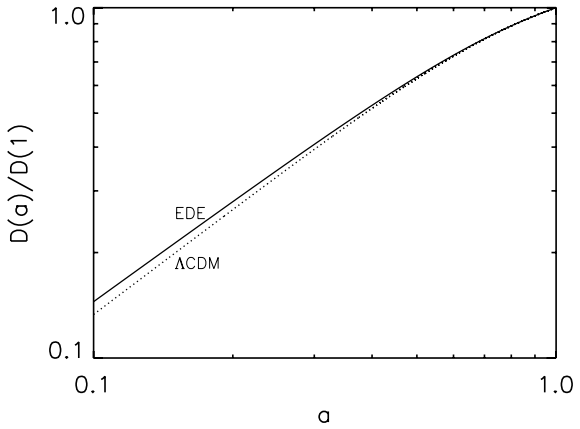

Figure 9. Growth factors for the WMAP-5 flat ΛCDM cosmology (dotted curve) and for the early dark energy (EDE) model assumed in this section for comparison (solid curve).

contribution to the energy density of the universe over a wide range of redshifts. The differences between EDE models and pure ΛCDM are particularly evident at high redshifts, when the former has been shown to influence the growth of the first cosmic structures both in the linear and in the nonlinear regime.

We consider here the EDE model proposed in Linder (2006) and recently constrained by Xia & Viel (2009, their model EDE1). We compare this model with the ΛCDM cosmology assumed until now. The differences in the growth factors for these two models are shown in Figure 9 (the difference in the Hubble parameter evolution is smaller).

We quantify the departure of the correlators predicted for the EDE model from the ΛCDM one using the following expression:

$$\Delta\chi^2 = \sum_i \frac{(\langle\delta\mathcal{F}^n\kappa\rangle_{\rm EDE} - \langle\delta\mathcal{F}^n\kappa\rangle_{\Lambda\rm CDM})^2}{\sigma^2_{{\rm EDE},i}}. \quad (33)$$

Table 6
Summary of the Estimated $\Delta\chi^2$ Between EDE and ΛCDM for Four Different Combinations of Future QSO and CMB Experiments Using the $\langle\delta\mathcal{F}^2\kappa\rangle$ Correlator

QSO Sample	CMB Experiment	$\Delta\chi^2$
1.6×10^5 (BOSS)	Planck	0.3364
1.6×10^5 (BOSS)	ACTPOL	1.429
1.0×10^6 (BigBOSS)	Planck	2.102
1.0×10^6 (BigBOSS)	ACTPOL	8.929

The results are shown in Figure 10 and are summarized in Table 6. In this case, the differences between EDE and ΛCDM are very limited and could only be appreciated with some significance with an advanced CMB experiment like ACTPOL and by increasing the number of spectroscopic QSOs with BigBOSS. However, it is worth stressing that the two models presented here are in perfect agreement with all the low-redshift probes and the large-scale structure measurements provided by galaxy power spectra, CMB, Type Ia supernovae (SNe) and Lyα forest. Therefore, possible departures from ΛCDM can be investigated only by exploiting the capabilities of this intermediate redshift regime with such correlations or with similar observables in this redshift range.

4. CONCLUSIONS

This work presents a detailed investigation of the cross-correlation signals between transmitted Lyα flux and the weak-lensing convergence of the CMB along the same line of sight. One of the motivations behind this work is that the Lyα forest has already been shown to be a powerful cosmological tool and novel ways of exploring and deepening the understanding of the flux/matter relation could significantly improve our knowledge

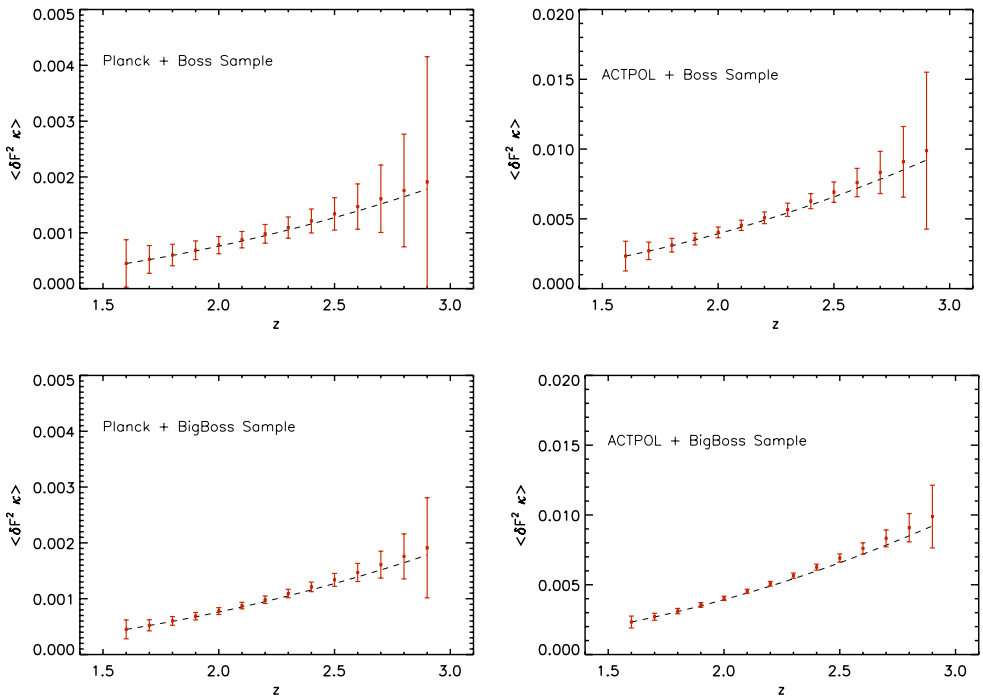

Figure 10. Value of $\langle\delta\mathcal{F}^2\kappa\rangle$ estimated for the early dark energy (EDE) model of Linder (2006). The dashed black line shows the expected value of the correlator for the ΛCDM cosmology assumed so far. Four different cases are reported here for Planck+BOSS (top left), Planck + BigBOSS (bottom left), ACTPOL+BOSS (top right), and ACTPOL+BigBOSS (bottom right). The redshift evolution of A is taken into account here.

(A color version of this figure is available in the online journal.)

of the high-redshift universe. These correlators are able to provide astrophysical and cosmological information: since they are sensitive to both the flux/matter relation and the value of cosmological parameters, in principle they can be used to put constraints on both.

The correlators investigated in the present work have a clear physical meaning. The correlation of $\delta\mathcal{F}$ with κ measures to what extent the fluctuations along the los mapped by the Lyα forest contribute to the CMB convergence field. This correlation is dominated by long-wavelength modes ($k \lesssim 10^{-1}\ h\,\mathrm{Mpc}^{-1}$) and as such is more sensitive to Lyα forest continuum fitting procedures. The correlation of the flux variance $\delta\mathcal{F}^2$ with κ measures to what extent the growth of short-wavelength modes (mapped by the Lyα flux) is enhanced or depressed by the fact that the latter are sitting in regions that are overdense or underdense on large scales. This interplay between short- and long-wavelength modes is well exemplified by the redshift dependence of the S/N ratio for $\langle\delta\mathcal{F}^2\kappa\rangle$: lowering the redshift increases the S/N because while the variance of $\langle\delta\mathcal{F}^2\kappa\rangle$ is dominated by the independent growth of long- and short-wavelength modes, the value of $\langle\delta\mathcal{F}^2\kappa\rangle$ itself receives an extra contribution due to the fact that the growth of the short-wavelength modes is enhanced by the presence (and independent growth) of the long-wavelength modes. Furthermore, this correlator is sensitive to intermediate-to-small scales ($k \gtrsim 10^{-2}\ h\,\mathrm{Mpc}^{-1}$) and as such it should be less sensitive to Lyα forest continuum fitting procedures.

To estimate the values of the correlators, their variance, and their S/Ns, we rely on linear theory and simple approximations, such as the fluctuating Gunn–Peterson approximation at first order. Although the framework is simplified, the results are by no means obvious since different modes enter non-trivially in these quantities and in their S/Ns. We estimate that such correlations may be detectable at a high significance level by Planck and the SDSS-III BOSS survey, experiments that are already collecting data. Moreover, our investigation of the modes of the Lyα forest that contribute to $\langle\delta\mathcal{F}^2\kappa\rangle$ shows that the low-resolution Lyα spectra measured by SDSS-III (which is aimed at the measurement of baryon acoustic oscillations at $z = 2$–4; McDonald & Eisenstein 2007; Slosar et al. 2009) should have enough resolution to yield a significant S/N.

The peculiar dependence of $\langle\delta\mathcal{F}^2\kappa\rangle$ on intermediate-to-short scales and its sensitivity to the value of the power spectrum normalization σ_8 makes it a very useful cosmological tool to test all models characterized by variations of the power spectrum on such scales. In particular, we applied our estimates to evaluate the sensitivity of $\langle\delta\mathcal{F}^2\kappa\rangle$ to changes in σ_8 due to variations in the sum of the neutrino masses and to show how promising this measurement could be in constraining the latter.

Finally, some caveats are in order. First, the code developed to estimate $\langle\delta\mathcal{F}^2\kappa\rangle$ and its variance is based on the tree-level perturbation theory results reported here. As such, the results shown do not take into account nonlinearities induced by gravitational collapse. The extension of the analytical results to take into account this aspect is actually quite straightforward, as it only requires the implementation of the so-called hyperextended perturbation theory for the bispectrum (Scoccimarro & Couchman 2001). However, the implementation of such changes in a numerical code is less trivial, as the integrations over the power spectrum and over the comoving distance cannot be factored any longer. We have nonetheless reason to speculate that the nonlinearities induced by gravitational collapse will not dramatically change the picture outlined here. At the redshift range spanned by the Lyα forest, nonlinearities are normally mild and confined to short scales. Furthermore, as shown in Section 2.5, the S/N for $\langle\delta\mathcal{F}^2\kappa\rangle$ is dominated by modes with $k \gtrsim 10^{-2}\ h\,\mathrm{Mpc}^{-1}$, but all decades above $10^{-2}\ h\,\mathrm{Mpc}^{-1}$ contribute in the same proportion to both the signal *and* its variance. It is therefore conceivable to filter out of the Lyα spectra the shortest scales, which are the most affected by nonlinearities, and still be able to retain a non-negligible S/N.

The second caveat pertains the estimate of the correlators' variance. It is in fact necessary to point out that to obtain such *estimates* Wick's theorem has been applied. Whether the use of Wick's theorem may or may not lead to an accurate result when considering the variance of $\langle\delta\mathcal{F}^2\kappa\rangle$ is debatable. On the one hand, it is possible to point out that the largest part of the signal arises at small separations, where the value of the correlator is dominated by its connected part. Analogously, it could be possible to argue that the use of Wick's theorem may lead to underestimating the correlators' variance. An exact evaluation of the variance of $\langle\delta\mathcal{F}^2\kappa\rangle$, however, requires the exact calculation of a six-point function, which to the best of our knowledge, has never been determined. On the other hand, it is also possible to point out that the connected part of $\langle\delta_c\delta_{c'}\delta_q^2\delta_{q'}^2\rangle$ will be significantly non-zero only when the distances between the different points are small. As such, this term will give a non-zero contribution proportional to the length of the Lyα spectrum, which should be subdominant with respect to the ones considered in Section 2.3 that are proportional to the distance from the observer all the way to the last scattering surface.

The third caveat pertains the expansion of the expression for the flux, Equation (1). Despite the fact that the expansion carried out in Equation (2) is correct on scales larger than about 1 h^{-1}Mpc, we point out here that the flux as expressed in Equation (1) is intrinsically a nonlinear function of the overdensity field. It is therefore reasonable to wonder whether the nonlinearities induced by this nonlinear mapping would somehow affect the conclusions presented here. A simple way to sidestep the present question is to undo the nonlinear mapping by defining a new observable $\hat{\mathcal{F}} = -\ln(\mathcal{F}) = A(1+\delta_{\mathrm{IGM}})^{\beta}$ and to proceed by measuring its correlations.

The best way to assess to what extent the above caveats affect the estimates reported in the present work is through numerical simulations, calculating the convergence field on a light cone and, at the same time measuring Lyα forest synthetic spectra and cross-correlating the two. This will be the next step in our investigation and the focus of the next publication.

Finally, on the analytical side we still need to address the estimate of the correlators when the power spectrum shows evolution in redshift *and* on different scales at the same time. As pointed out, $\langle\delta\mathcal{F}^2\kappa\rangle$ is sensitive to scales $k \gtrsim 10^{-2}\ h\,\mathrm{Mpc}^{-1}$. As such this correlator is an ideal tool to test modifications of gravity that show scale-dependent growth. At the same time, this development would also allow the implementation of the hyperextended perturbation theory results and as such to address analytically the impact of gravity-induced nonlinearities on the value of the correlators.

We thank S. Matarrese, F. Bernardeau, S. Dodelson, J. Frieman, E. Sefusatti, N. Gnedin, R. Scoccimarro, S. Ho, D. Weinberg, and J. P. Uzan for useful conversations. We also thank the referee for a constructive report. A.V. is supported by the DOE at Fermilab. M.V. is supported by grants INFN/PD51, ASI-AAE a PRIN MIUR, a PRIN INAF 2009, and the ERC-StG "cosmoIGM." D.N.S. and S.D. are supported by NSF grant

AST/0707731 and NASA theory grant NNX08AH30G. D.N.S. thanks the APC (Paris) for its hospitality during the spring of 2008 when this project was initiated. A.V. thanks IAP (Paris) for hospitality during different stages of this project.

APPENDIX

DERIVATION OF PERTURBATIVE RESULTS FOR $\langle \delta\mathcal{F}^2\,\kappa\rangle$

In this appendix, we derive the expression for $\langle \delta\mathcal{F}^2\,\kappa\rangle$ shown in the text, Equations (19)–(21). We move from Equation (5) and need to find an efficient way to evaluate $\langle \delta^2(\hat{n},\chi_q)\delta(\hat{n},\chi_c)\rangle$. We start by Fourier transforming this cumulant correlator to get

$$\begin{aligned}\langle \delta_q^2\delta_c\rangle &= \int \frac{d^3\vec{k}_1}{(2\pi)^3}\frac{d^3\vec{k}_2}{(2\pi)^3}\frac{d^3\vec{k}_3}{(2\pi)^3}\, e^{i[(\vec{k}_1+\vec{k}_2)\cdot\vec{x}_q+\vec{k}_3\cdot\vec{x}_c]}\, W_\alpha(k_{1,\parallel})W_\alpha(k_{2,\parallel})W_\kappa(k_{3,\perp})\langle\delta(\vec{k}_1)\delta(\vec{k}_2)\delta(\vec{k}_3)\rangle\\ &= \int \frac{d^3\vec{k}_1}{(2\pi)^3}\frac{d^3\vec{k}_2}{(2\pi)^3}\frac{d^3\vec{k}_3}{(2\pi)^3}\, e^{i[(\vec{k}_1+\vec{k}_2)\cdot\vec{x}_q+\vec{k}_3\cdot\vec{x}_c]}\,(2\pi)^3\delta_D^3(\vec{k}_1+\vec{k}_2+\vec{k}_3)W_\alpha(k_{1,\parallel})W_\alpha(k_{2,\parallel})W_\kappa(k_{3,\perp})B(\vec{k}_1,\vec{k}_2,\vec{k}_3)\\ &= \int \frac{d^3\vec{k}_1}{(2\pi)^3}\frac{d^3\vec{k}_2}{(2\pi)^3}\frac{d^3\vec{k}_3}{(2\pi)^3}\, e^{i[(\vec{k}_1+\vec{k}_2)\cdot\vec{x}_q+\vec{k}_3\cdot\vec{x}_c]}\,(2\pi)^3\delta_D^3(\vec{k}_1+\vec{k}_2+\vec{k}_3)W_\alpha(k_{1,\parallel})W_\alpha(k_{2,\parallel})W_\kappa(k_{3,\perp})\\ &\quad\times 2[\,F_2(\vec{k}_1,\vec{k}_2)P_L(\vec{k}_1,\chi_1)\,P_L(\vec{k}_2,\chi_2)+\,F_2(\vec{k}_2,\vec{k}_3)P_L(\vec{k}_2,\chi_2)\,P_L(\vec{k}_3,\chi_3)+F_2(\vec{k}_3,\vec{k}_1)P_L(\vec{k}_3,\chi_3)\,P_L(\vec{k}_1,\chi_1)].\end{aligned} \tag{A1}$$

In the second line, we introduced the bispectrum $B(\vec{k}_1,\vec{k}_2,\vec{k}_3)$, while in the third line we replaced the bispectrum with the expression for its kernel F_2 and products of the linear matter power spectrum $P_L(\vec{k},\chi)$. For the sake of brevity, we keep implicit the dependence of the window functions on the cutoff scales: $W_\alpha(k_{i,\parallel}) = W_\alpha(k_{i,\parallel},k_L,k_l)$ and $W_\kappa(\vec{k}_{i,\perp}) = W_\kappa(\vec{k}_{i,\perp},k_C)$. Next, we point out that the evaluation of Equation (A1) requires in general the integration over a six-dimensional k-space, which is further complicated by the fact that the different window functions break the spherical symmetry that one would normally exploit.

In what follows we adopt the tree-level approximation to the bispectrum kernel,

$$F_2(\vec{k}_i,\vec{k}_j) = \frac{5}{7} + \frac{1}{2}\frac{\vec{k}_i\cdot\vec{k}_j}{k_i^2\,k_j^2}\left(k_i^2+k_j^2\right) + \frac{2}{7}\left(\frac{\vec{k}_i\cdot\vec{k}_j}{k_i\,k_j}\right)^2, \tag{A2}$$

which can readily be obtained from the more general expression derived by Scoccimarro & Couchman (2001):

$$F_2^{\rm HEPT}(\vec{k}_i,\vec{k}_j) = \frac{5}{7}\,a(n,k_i)\,a(n,k_j) + \frac{1}{2}\frac{\vec{k}_i\cdot\vec{k}_j}{k_i^2\,k_j^2}\left(k_i^2+k_j^2\right)b(n,k_i)\,b(n,k_j) + \frac{2}{7}\left(\frac{\vec{k}_i\cdot\vec{k}_j}{k_i\,k_j}\right)^2 c(n,k_i)\,c(n,k_j), \tag{A3}$$

setting the three auxiliary functions $a(k)$, $b(k)$, and $c(k)$ that allow us to account for nonlinear growth of structure equal to unity. A generalization of the results shown below to take into account the more general formulation of Equation (A3) is straightforward to derive.

To proceed further, we note that each of the three terms appearing in the square bracket of Equation (A1) depends only on *two* of the three wavevectors. When moving from the second to the third line, it is then essential *not* to carry out the integration over the delta function, because for *each* of these terms we integrate the Dirac δ in order to obtain an expression that depends only on the same wavevectors that appear in the F_2 kernel. The fact that two of the three physical points are the same also spoils the cyclic symmetry of the bispectrum. In particular, the {1, 2} term will differ from the {2, 3} and {3, 1} terms. We therefore let

$$\left\langle \delta_q^2\delta_c\right\rangle = \left\langle \delta_q^2\delta_c\right\rangle_{1,2} + 2\left\langle \delta_q^2\delta_c\right\rangle_{2,3} \tag{A4}$$

and start by considering $\langle\delta_q^2\delta_c\rangle_{1,2}$. Integrating over the δ_D function in order to get rid of $\vec{k}_3$ in favor of $\vec{k}_1$ and $\vec{k}_2$ and then adopting a cylindrical coordinate system in k-space, we get

$$\begin{aligned}\langle\delta^2\delta\rangle_{1,2} &= 2\int \frac{dk_{1,\parallel}}{2\pi}\frac{dk_{2,\parallel}}{2\pi}e^{i(k_{1,\parallel}+k_{2,\parallel})\Delta\chi}\,W_\alpha(k_{1,\parallel})\,W_\alpha(k_{2,\parallel})\int_{|k_{1,\parallel}|}^\infty\frac{k_1dk_1}{(2\pi)^2}P(\vec{k}_1,\chi_1)\int_{|k_{2,\parallel}|}^\infty\frac{k_2dk_2}{(2\pi)^2}P(\vec{k}_2,\chi_2)\\ &\quad\times\int d\phi\int d\theta_\perp F_2(\vec{k}_1,\vec{k}_2)\,W_\kappa[|\vec{k}_{1,\perp}+\vec{k}_{2,\perp}|].\end{aligned} \tag{A5}$$

As also recognized by Bernardeau (1996), the most challenging part of the calculation consists of the integration over the angular variables. This is because the convergence window function depends on $|\vec{k}_{1,\perp}+\vec{k}_{2,\perp}|$. The integration over the angular variables in this case does not necessarily lead to an expression that may be numerically efficient to evaluate. In particular, we aim to keep integrations factored as much as possible. Our first goal then is to integrate

$$\begin{aligned}\int d\phi\int d\theta_\perp F_2(\vec{k}_1,\vec{k}_2)\,W_\kappa[|\vec{k}_{1,\perp}+\vec{k}_{2,\perp}|] &= 2\pi\,\exp\left(-\frac{k_{1,\perp}^2}{k_C^2}\right)\exp\left(-\frac{k_{2,\perp}^2}{k_C^2}\right)\\ &\quad\times\int d\theta_\perp F_2(\vec{k}_1,\vec{k}_2)\,\exp\left[-2\frac{k_{1,\perp}k_{2,\perp}\cos(\theta_\perp)}{k_C^2}\right],\end{aligned} \tag{A6}$$

where $\theta_\perp$ is the angle between $\vec{k}_{1,\perp}$ and $\vec{k}_{2,\perp}$. Now, as far as the integration over the angular variable is concerned, the kernel F_2 can be written as

$$F_2(\vec{k}_1, \vec{k}_2) = R + S\,\cos(\theta_\perp) + T\,\cos^2(\theta_\perp), \tag{A7}$$

where we have decomposed $\vec{k}$ into its components parallel and perpendicular to the los according to $\vec{k} = k_\parallel \hat{n} + \vec{k}_\perp$ and extracted the terms that are proportional to different powers of $\cos(\theta_\perp)$:

$$R = \frac{5}{7} + \frac{1}{2}\frac{k_{1,\parallel}\,k_{2,\parallel}}{k_1^2\,k_2^2}\left(k_1^2 + k_2^2\right) + \frac{2}{7}\left(\frac{k_{1,\parallel}\,k_{2,\parallel}}{k_1\,k_2}\right)^2, \tag{A8}$$

$$S = \frac{1}{2}\frac{k_{1,\perp}\,k_{2,\perp}}{k_1^2\,k_2^2}\left(k_1^2 + k_2^2\right) + \frac{4}{7}\frac{k_{1,\parallel}\,k_{2,\parallel}\,k_{1,\perp}\,k_{2,\perp}}{k_1^2\,k_2^2}, \tag{A9}$$

$$T = \frac{2}{7}\left(\frac{k_{1,\perp}\,k_{2,\perp}}{k_1\,k_2}\right)^2. \tag{A10}$$

Integration over the angular variable can then be carried out by remembering that

$$\int_0^{2\pi} d\theta\,\exp\left[-\alpha\cos(\theta)\right] = 2\pi\,I_0(\alpha), \tag{A11}$$

$$\int_0^{2\pi} d\theta\,\exp\left[-\alpha\cos(\theta)\right]\cos(\theta) = -2\pi\,I_1(\alpha), \tag{A12}$$

$$\int_0^{2\pi} d\theta\,\exp\left[-\alpha\cos(\theta)\right]\cos^2(\theta) = \frac{2\pi}{\alpha}\left[I_1(\alpha) + \alpha\,I_2(\alpha)\right], \tag{A13}$$

where I_n denotes the modified Bessel function of the first kind and nth order. The integration over the angular variables yields

$$\int d\phi \int d\theta_\perp F_2(\vec{k}_1, \vec{k}_2)\,W_C[|\vec{k}_{1,\perp} + \vec{k}_{2,\perp}|] = (2\pi)^2\,\exp\left(-\frac{k_{1,\perp}^2}{k_C^2}\right)\exp\left(-\frac{k_{2,\perp}^2}{k_C^2}\right)$$
$$\times\left\{R\,I_0\left(2\frac{k_{1,\perp}k_{2,\perp}}{k_C^2}\right) - S\,I_1\left(2\frac{k_{1,\perp}k_{2,\perp}}{k_C^2}\right) + T\left[\frac{k_C^2}{2\,k_{1,\perp}k_{2,\perp}}I_1\left(2\frac{k_{1,\perp}k_{2,\perp}}{k_C^2}\right) + I_2\left(2\frac{k_{1,\perp}k_{2,\perp}}{k_C^2}\right)\right]\right\}.$$

The difficulty with this result is that every term depends on the product $k_{1,\perp}k_{2,\perp}$. As such, we are facing a two-dimensional *joint* integration over the whole $[k_{1,\perp}, k_{2,\perp}]$ domain. If on the one hand this is doable, on the other hand we are more interested in obtaining a final result which is a product of integrals instead of the integral of the product. It is possible to move around this obstacle recalling that (Abramowitz & Stegun 1965, Equation (9.6.10)),

$$I_\nu(z) = \sum_{n=0}^{\infty}\frac{1}{n!\Gamma(\nu+n+1)}\left(\frac{z}{2}\right)^{2n+\nu} = \sum_{n=0}^{\infty} I_\nu^{(n)}\left(\frac{z}{2}\right)^{2n+\nu}. \tag{A14}$$

We can write the modified Bessel function splitting the dependence on $k_{1,\perp}$ and $k_{2,\perp}$ as

$$I_0\left(2\frac{k_{1,\perp}k_{2,\perp}}{k_C^2}\right) = \sum_{n=0}^{\infty} I_0^{(n)}\left(\frac{k_{1,\perp}^2}{k_C^2}\right)^n\left(\frac{k_{2,\perp}^2}{k_C^2}\right)^n, \tag{A15}$$

$$I_1\left(2\frac{k_{1,\perp}k_{2,\perp}}{k_C^2}\right) = \frac{k_{1,\perp}k_{2,\perp}}{k_C^2}\sum_{n=0}^{\infty} I_1^{(n)}\left(\frac{k_{1,\perp}^2}{k_C^2}\right)^n\left(\frac{k_{2,\perp}^2}{k_C^2}\right)^n, \tag{A16}$$

$$I_2\left(2\frac{k_{1,\perp}k_{2,\perp}}{k_C^2}\right) = \left(\frac{k_{1,\perp}k_{2,\perp}}{k_C^2}\right)^2\sum_{n=0}^{\infty} I_2^{(n)}\left(\frac{k_{1,\perp}^2}{k_C^2}\right)^n\left(\frac{k_{2,\perp}^2}{k_C^2}\right)^n, \tag{A17}$$

where for the sake of brevity we use the following notation for the coefficients:

$$I_0^{(n)} = \frac{1}{n!^2}, \tag{A18}$$

$$I_1^{(n)} = \frac{1}{n!(n+1)!} = \frac{I_0^{(n)}}{n+1}, \tag{A19}$$

$$I_2^{(n)} = \frac{1}{n!(n+2)!} = \frac{I_0^{(n)}}{(n+1)(n+2)}. \tag{A20}$$

Now, however complicated, this form allows us to factor the different integrals. Let us start by considering the term $R\, I_0$. We have

$$\begin{aligned} R\, I_0 &= \sum_{m=0}^{\infty} I_0^{(m)} \left(\frac{k_{1,\perp}^2}{k_C^2}\right)^m \left(\frac{k_{2,\perp}^2}{k_C^2}\right)^m \left[\frac{5}{7} + \frac{1}{2}\frac{k_{1,\parallel}\, k_{2,\parallel}}{k_1^2\, k_2^2}\left(k_1^2 + k_2^2\right) + \frac{2}{7}\left(\frac{k_{1,\parallel}\, k_{2,\parallel}}{k_1\, k_2}\right)^2\right] \\ &= \sum_{m=0}^{\infty} I_0^{(m)} \left(\frac{k_1^2 - k_{1,\parallel}^2}{k_C^2}\right)^m \left(\frac{k_2^2 - k_{2,\parallel}^2}{k_C^2}\right)^m \frac{5}{7} \\ &\quad + \sum_{m=0}^{\infty} I_0^{(m)} \left(\frac{k_1^2 - k_{1,\parallel}^2}{k_C^2}\right)^m \left(\frac{k_2^2 - k_{2,\parallel}^2}{k_C^2}\right)^m \left[\frac{1}{2}\frac{k_{1,\parallel}\, k_{2,\parallel}}{k_1^2\, k_2^2}\left(k_1^2 + k_2^2\right)\right] \\ &\quad + \sum_{m=0}^{\infty} I_0^{(m)} \left(\frac{k_1^2 - k_{1,\parallel}^2}{k_C^2}\right)^m \left(\frac{k_2^2 - k_{2,\parallel}^2}{k_C^2}\right)^m \left[\frac{2}{7}\left(\frac{k_{1,\parallel}\, k_{2,\parallel}}{k_1\, k_2}\right)^2\right], \end{aligned} \tag{A21}$$

where in going from the first to the second step we expressed $k_\perp^2$ as a function of k and $k_\parallel$ using the fact that $k^2 = k_\parallel^2 + k_\perp^2$. This is necessary because the power spectrum is function of k and not of $k_\perp$. We can then proceed by defining the following functions:

$$\tilde{H}_m(k_\parallel, \chi; k_C) \equiv \int_{|k_\parallel|}^{\infty} \frac{k\, dk}{2\pi} \sqrt{I_0^{(m)}}\, P(k, \chi) \left(\frac{k^2 - k_\parallel^2}{k_C^2}\right)^m \exp\left(-\frac{k^2 - k_\parallel^2}{k_C^2}\right), \tag{A22}$$

$$\tilde{L}_m(k_\parallel, \chi; k_C) \equiv \int_{|k_\parallel|}^{\infty} \frac{dk}{2\pi k} \sqrt{I_0^{(m)}}\, P(k, \chi) \left(\frac{k^2 - k_\parallel^2}{k_C^2}\right)^m \exp\left(-\frac{k^2 - k_\parallel^2}{k_C^2}\right). \tag{A23}$$

It is important to note that because of the integration domain *all* the above functions are *even* in $k_\parallel$, regardless of the value of m. With the help of these functions, we then have

$$\begin{aligned} &\int_{|k_{1,\parallel}|}^{\infty} \frac{k_1 dk_1}{(2\pi)^2} P(\vec{k}_1, \chi_1) \int_{|k_{2,\parallel}|}^{\infty} \frac{k_2 dk_2}{(2\pi)^2} P(\vec{k}_2, \chi_2) \int d\phi \int d\theta_\perp R\, W_\kappa[|\vec{k}_{1,\perp} + \vec{k}_{2,\perp}|] \\ &= \frac{5}{7}\sum_{m=0}^{\infty} \tilde{H}_m(k_{1,\parallel}, \chi_1)\tilde{H}_m(k_{2,\parallel}, \chi_2) + \frac{2\, k_{1,\parallel}^2\, k_{2,\parallel}^2}{7} \sum_{m=0}^{\infty} \tilde{L}_m(k_{1,\parallel}, \chi_1)\tilde{L}_m(k_{2,\parallel}, \chi_2) \\ &\quad + \frac{k_{1,\parallel}\, k_{2,\parallel}}{2}\left[\sum_{m=0}^{\infty} \tilde{H}_m(k_{1,\parallel}, \chi_1)\tilde{L}_m(k_{2,\parallel}, \chi_2) + \sum_{m=0}^{\infty} \tilde{L}_m(k_{1,\parallel}, \chi_1)\tilde{H}_m(k_{2,\parallel}, \chi_2)\right]. \end{aligned} \tag{A24}$$

We have therefore succeeded in obtaining an expression that has the dependence on $k_{1,\parallel}$ and $k_{2,\parallel}$ *completely factored*. The sums over m and the fact that each term is a product of factors that only depend either on $k_{1,\parallel}$ or on $k_{2,\parallel}$ allow an integration term by term and at the same time to bypass the two-dimensional joint integration.

We can then proceed exactly in the same way for the other two terms, $S\, I_1$ and $T\, I_2$, with the only difference that in order to obtain expressions where only the coefficients of the modified Bessel function of 0th order $I_0^{(m)}$ appear we use the fact that $I_1^{(m)} = (m+1)\, I_0^{(m+1)}$. We then obtain for the S term the following expression:

$$\begin{aligned} &\int_{|k_{1,\parallel}|}^{\infty} \frac{k_1 dk_1}{(2\pi)^2} P(\vec{k}_1, \chi_1) \int_{|k_{2,\parallel}|}^{\infty} \frac{k_2 dk_2}{(2\pi)^2} P(\vec{k}_2, \chi_2) \int d\phi \int d\theta_\perp S\, \cos(\theta_\perp)\, W_\kappa[|\vec{k}_{1,\perp} + \vec{k}_{2,\perp}|] \\ &= -\frac{k_C^2}{2}\sum_{m=0}^{\infty} m\, [\tilde{H}_m(k_{1,\parallel}, \chi_1)\tilde{L}_m(k_{2,\parallel}, \chi_2) + \tilde{L}_m(k_{1,\parallel}, \chi_1)\tilde{H}_m(k_{2,\parallel}, \chi_2)] - \frac{4\, k_C^2\, k_{1,\parallel}\, k_{2,\parallel}}{7} \sum_{m=0}^{\infty} m\, \tilde{L}_m(k_{1,\parallel}, \chi_1)\tilde{L}_m(k_{2,\parallel}, \chi_2). \end{aligned} \tag{A25}$$

Finally, the T term gives

$$\int_{|k_{1,\parallel}|}^{\infty} \frac{k_1 dk_1}{(2\pi)^2} P(\vec{k}_1, \chi_1) \int_{|k_{2,\parallel}|}^{\infty} \frac{k_2 dk_2}{(2\pi)^2} P(\vec{k}_2, \chi_2) \int d\phi \int d\theta_\perp T \cos^2(\theta_\perp) W_C[|\vec{k}_{1,\perp} + \vec{k}_{2,\perp}|]$$
$$= \frac{k_C^4}{7} \sum_{m=0}^{\infty} m(2m-1) \tilde{L}_m(k_{1,\parallel}, \chi_1) \tilde{L}_m(k_{2,\parallel}, \chi_2). \tag{A26}$$

With the introduction of the definitions (Equations (A22)–(A23)) and with the series expansion for the modified Bessel function, we have therefore managed to carry out the integration over the perpendicular part of the wavevector. We are then left with the integration over $k_\parallel$. First recall that the window functions acting on the Lyα flux are

$$W_\alpha(k_\parallel, k_L, k_l) \equiv [1 - e^{-(k_\parallel/k_l)^2}] e^{-(k_\parallel/k_L)^2} = e^{-(k_\parallel/k_L)^2} - e^{-(k_\parallel/\bar{k})^2} \tag{A27}$$

and that in Equation (A5) they decouple from one another. We can proceed further by defining the following function:

$$f_m^{(n)}(\Delta\chi, \chi; k_C, k_L) \equiv \int_{-\infty}^{\infty} \frac{dk_\parallel}{2\pi} \left(\frac{k_\parallel}{k_L}\right)^n \exp\left[-\frac{k_\parallel^2}{k_L^2} + ik_\parallel \Delta\chi\right] \tilde{f}_m(k_\parallel, \chi; k_C), \tag{A28}$$

where $f = \{H, L\}$. It is straightforward to note that because all the tilde functions are even in $k_\parallel$, depending on the value of n the above Fourier transforms are either purely real (if n is even) or purely imaginary (if n is odd). Furthermore, if n is even the above functions are *real* and *even*, while if n is odd the above functions are *imaginary* and *odd*. Carrying out the integration on $k_\parallel$ is then straightforward, as it just corresponds the replacement $k_\parallel^n \tilde{f}_m(k_\parallel, \chi; k_C) \to k_L^n f_m^{(n)}(\Delta\chi, \chi; k_C, k_L) - \bar{k}^n f_m^{(n)}(\Delta\chi, \chi; k_C, \bar{k})$. Finally, from a computational point of view this approach is rather efficient, as the tilded function need to be calculated only once and then used to construct the two-index functions.

With the help of these auxiliary functions, we can finally obtain the following expression for the cumulant correlator $\langle\delta^2\delta\rangle_{1,2}$:

$$\begin{aligned}
\langle\delta^2\delta\rangle_{1,2} = 2\sum_{m=0}^{\infty} \Bigg\{ & \frac{5}{7}\left[H_m^{(0)}(\Delta\chi, \chi_q; k_C, k_L) - H_m^{(0)}(\Delta\chi, \chi_q; k_C, \bar{k})\right]^2 \\
& + \left[k_L H_m^{(1)}(\Delta\chi, \chi_q; k_C, k_L) - \bar{k} H_m^{(1)}(\Delta\chi, \chi_q; k_C, \bar{k})\right]\left[k_L L_m^{(1)}(\Delta\chi, \chi_q; k_C, k_L) - \bar{k} L_m^{(1)}(\Delta\chi, \chi_q; k_C, \bar{k})\right] \\
& - m k_C^2 \left[H_m^{(0)}(\Delta\chi, \chi_q; k_C, k_L) - H_m^{(0)}(\Delta\chi, \chi_q; k_C, \bar{k})\right]\left[L_m^{(0)}(\Delta\chi, \chi_q; k_C, k_L) - L_m^{(0)}(\Delta\chi, \chi_q; k_C, \bar{k})\right] \\
& + \frac{2}{7}\left[k_L^2 L_m^{(2)}(\Delta\chi, \chi_q; k_C, k_L) - \bar{k}^2 L_m^{(2)}(\Delta\chi, \chi_q; k_C, \bar{k})\right]^2 \\
& - \frac{4m}{7} k_C^2 \left[k_L L_m^{(1)}(\Delta\chi, \chi_q; k_C, k_L) - \bar{k} L_m^{(1)}(\Delta\chi, \chi_q; k_C, \bar{k})\right]^2 \\
& + \frac{m(2m-1)}{7} k_C^4 \left[L_m^{(0)}(\Delta\chi, \chi_q; k_C, k_L) - L_m^{(0)}(\Delta\chi, \chi_q; k_C, \bar{k})\right]^2 \Bigg\}.
\end{aligned} \tag{A29}$$

A cautionary note is in order. As mentioned above, the functions defined through Equation (A28) are purely imaginary if the index (n) is odd. However, note that in Equation (A29) above there are always two such functions that appear together (as in the case with $H_m^{(1)} L_m^{(1)}$), thus ensuring that $\langle\delta^2\delta\rangle_{1,2}$ is always real valued.

Let us now move to calculate $\langle\delta^2\delta\rangle_{2,3}$. Note incidentally that this term is exactly equal to $\langle\delta^2\delta\rangle_{3,1}$. We start from the now usual expression

$$\begin{aligned}
\langle\delta^2\delta\rangle_{2,3} = 2 \int \frac{dk_{2,\parallel}}{2\pi} \frac{dk_{3,\parallel}}{2\pi} e^{-i k_{3,\parallel}\Delta\chi} W_\alpha(-k_{2,\parallel} - k_{3,\parallel}) W_\alpha(k_{2,\parallel}) \int_{|k_{2,\parallel}|}^{\infty} \frac{k_2 dk_2}{(2\pi)^2} P(\vec{k}_2, \chi_2) \int_{|k_{3,\parallel}|}^{\infty} \frac{k_3 dk_3}{(2\pi)^2} P(\vec{k}_3, \chi_3) \\
\times \int d\phi \int d\theta_\perp F_2(\vec{k}_2, \vec{k}_3) W_\kappa(\vec{k}_{3,\perp}),
\end{aligned} \tag{A30}$$

where, as previously, we have traded the integrations over $k_{i,\perp}$ for the ones over k_i. In this case, the integration over the angular variables does not pose any problem as the window function W_κ is actually a function of $k_{3,\perp}$ only and it can be safely pulled out of the angular integrals:

$$\int d\phi \int d\theta_\perp F_2(\vec{k}_2, \vec{k}_3) = \frac{(2\pi)^2}{7}(5+1) + \frac{(2\pi)^2}{2} k_{2,\parallel} k_{3,\parallel} \left(\frac{1}{k_2^2} + \frac{1}{k_3^2}\right) + \frac{(2\pi)^2}{7}\left[3\frac{k_{2,\parallel}^2 k_{3,\parallel}^2}{k_2^2 k_3^2} - \left(\frac{k_{2,\parallel}^2}{k_2^2} + \frac{k_{3,\parallel}^2}{k_3^2}\right)\right]. \tag{A31}$$

It is here necessary to point out that since W_κ depends only on $k_{3,\perp}$, the tilded functions that will appear when the integration over k_2 is carried out will contain no filter function. We characterize this function by substituting to k_C the ∞ symbol, as to all extent the

Gaussian filter with $k_C \to \infty$ just yields unity. We then have

$$\begin{aligned}
&\int_{|k_{2,\parallel}|}^{\infty} \frac{k_2 dk_2}{(2\pi)^2} P(\vec{k}_2, \chi_2) \int_{|k_{3,\parallel}|}^{\infty} \frac{k_3 dk_3}{(2\pi)^2} P(\vec{k}_3, \chi_3) \int d\phi \int d\theta_\perp F_2(\vec{k}_2, \vec{k}_3)\, W_\kappa(\vec{k}_{3,\perp}) \\
&= \int_{|k_{2,\parallel}|}^{\infty} \frac{k_2 dk_2}{(2\pi)^2} P(\vec{k}_2, \chi_2) \int_{|k_{3,\parallel}|}^{\infty} \frac{k_3 dk_3}{(2\pi)^2} P(\vec{k}_3, \chi_3) \exp\left(-\frac{k_3^2 - k_{3,\parallel}^2}{k_C^2}\right) \\
&\quad \times (2\pi)^2 \left[\frac{5}{7} + \frac{1}{2}\, k_{2,\parallel}\, k_{3,\parallel} \left(\frac{1}{k_2^2} + \frac{1}{k_3^2}\right) + \frac{1}{7}\, \frac{1}{k_2^2 k_3^2} \left(2\, k_{2,\parallel}^2\, k_{3,\parallel}^2 + k_{2,\perp}^2\, k_{3,\perp}^2\right)\right] \\
&= \frac{6}{7}\, \tilde{H}_0(k_{2,\parallel}, \chi_2; \infty) \tilde{H}_0(k_{3,\parallel}, \chi_3; k_C) + \frac{1}{2}\, k_{2,\parallel}\, k_{3,\parallel} \tilde{L}_0(k_{2,\parallel}, \chi_2; \infty) \tilde{H}_0(k_{3,\parallel}, \chi_3; k_C) \\
&\quad + \frac{1}{2}\, k_{2,\parallel}\, k_{3,\parallel} \tilde{H}_0(k_{2,\parallel}, \chi_2; \infty) \tilde{L}_0(k_{3,\parallel}, \chi_3; k_C) + \frac{3}{7}\, k_{2,\parallel}^2\, k_{3,\parallel}^2 \tilde{L}_0(k_{2,\parallel}, \chi_2; \infty) \tilde{L}_0(k_{3,\parallel}, \chi_3; k_C) \\
&\quad - \frac{1}{7} k_{3,\parallel}^2\, \tilde{H}_0(k_{2,\parallel}, \chi_2; \infty)\, \tilde{L}_0(k_{3,\parallel}, \chi_3; k_C) - \frac{1}{7} k_{2,\parallel}^2\, \tilde{L}_0(k_{2,\parallel}, \chi_2; \infty) \tilde{H}_0(k_{3,\parallel}, \chi_3; k_C).
\end{aligned} \tag{A32}$$

The expression for the window function acting on the Lyα flux is in this case:

$$\begin{aligned}
W_\alpha(-k_{2,\parallel} - k_{3,\parallel})\, W_\alpha(k_{2,\parallel}) &= \left[1 - e^{-\left(\frac{k_{2,\parallel}+k_{3,\parallel}}{k_I}\right)^2}\right] e^{-\left(\frac{k_{2,\parallel}+k_{3,\parallel}}{k_L}\right)^2} \left[1 - e^{-\left(\frac{k_{2,\parallel}}{k_I}\right)^2}\right] e^{-\left(\frac{k_{2,\parallel}}{k_L}\right)^2} \\
&= e^{-k_{3,\parallel}^2/k_L^2} \left(e^{-2k_{2,\parallel}^2/k_L^2} - e^{-k_{2,\parallel}^2/\hat{k}^2}\right) \sum_n \frac{(-2)^n}{n!} \left(\frac{k_{2,\parallel}}{k_L}\right)^n \left(\frac{k_{3,\parallel}}{k_L}\right)^n \\
&\quad + e^{-k_{3,\parallel}^2/\bar{k}^2} \left(e^{-2k_{2,\parallel}^2/\bar{k}^2} - e^{-k_{2,\parallel}^2/\hat{k}^2}\right) \sum_n \frac{(-2)^n}{n!} \left(\frac{k_{2,\parallel}}{\bar{k}}\right)^n \left(\frac{k_{3,\parallel}}{\bar{k}}\right)^n,
\end{aligned} \tag{A33}$$

where we have recast the window function in a combination that is suitable for furthering the calculation. Note in fact that the first and second terms in the sum differ only by the presence of k_L or $\bar{k}$ in the denominators of the exponentials. Furthermore, the terms in square brackets are functions of $k_{2,\parallel}$ only. We then define the coefficients

$$\bar{f}_m^{(n)}(\chi; k_L) \equiv \int_{-\infty}^{\infty} \frac{dk_\parallel}{2\pi} \left(\frac{k_\parallel}{k_L}\right)^n [e^{-2k_\parallel^2/k_L^2} - e^{-k_\parallel^2/\hat{k}^2}] \tilde{f}_m(k_\parallel, \chi, \infty), \tag{A34}$$

$$\bar{f}_m^{(n)}(\chi; \bar{k}) \equiv \int_{-\infty}^{\infty} \frac{dk_\parallel}{2\pi} \left(\frac{k_\parallel}{\bar{k}}\right)^n [e^{-2k_\parallel^2/\bar{k}^2} - e^{-k_\parallel^2/\hat{k}^2}] \tilde{f}_m(k_\parallel, \chi, \infty). \tag{A35}$$

A point worth making is that the second expression can be obtained from the first one with the substitution $k_L \to \bar{k}$ in the denominators but *not* in the expression for $\hat{k}$, hence the necessity for two separate definitions. Considering then the following generic term, it is possible to show that

$$\begin{aligned}
&\int \frac{dk_2}{2\pi} \frac{dk_3}{2\pi}\, k_2^p\, k_3^q\, \tilde{f}_i(k_2, \chi_2; \infty) \tilde{g}_j(k_3, \chi_3; k_C) W_\alpha(-k_2 - k_3)\, W_\alpha(k_2)\, e^{-ik_3 \Delta\chi} \\
&= \sum_m \frac{(-2)^m}{m!} \left[k_L^{(p+q)} g_j^{(q+m)}(\Delta\chi, \chi; k_C, k_L) \bar{f}_i^{(p+m)}(\chi_2, k_L) + \bar{k}^{(p+q)} g_j^{(q+m)}(\Delta\chi, \chi; k_C, \bar{k}) \bar{f}_i^{(p+m)}(\chi_2, \bar{k})\right],
\end{aligned} \tag{A36}$$

which then leads directly to

$$\begin{aligned}
\langle \delta_q^2 \delta_c \rangle_{2,3} = 2 \sum_{m=0}^{\infty} \frac{(-1)^m\, 2^m}{m!} \Bigg[&\frac{6}{7} \bar{H}_0^{(m)}(k_L) H_0^{(m)}(\Delta\chi; k_C, k_L) + \frac{1}{2} k_L^2 \bar{L}_0^{(m+1)}(k_L)\, H_0^{(m+1)}(\Delta\chi; k_C, k_L) \\
&+ \frac{1}{2} k_L^2 \bar{H}_0^{(m+1)}(k_L)\, L_0^{(m+1)}(\Delta\chi; k_C, k_L) + \frac{3}{7} k_L^4\, \bar{L}_0^{(m+2)}(k_L)\, L_0^{(m+2)}(\Delta\chi; k_C, k_L) \\
&- \frac{k_L^2}{7} \bar{H}_0^{(m)}(k_L)\, L_0^{(m+2)}(\Delta\chi; k_C, k_L) - \frac{k_L^2}{7} \bar{L}_0^{(m+2)}(k_L)\, H_0^{(m)}(\Delta\chi; k_C, k_L) + (k_L \to \bar{k})\Bigg].
\end{aligned} \tag{A37}$$

Note that in the above expression that while $\bar{f}_m^{(n)}$ are always real, $f_m^{(n)}$ can be real or imaginary depending on whether n is even or odd. However, the fact that $\bar{f}_m^{(n)}$ is zero whenever the upper index is odd guarantees that $\langle \delta^2 \delta \rangle_{2,3}$ is always real valued. Also, note that while the coefficients $\bar{f}_m^{(n)}(\chi_Q; k_L)$ are decreasing with m, the coefficients $\bar{f}_m^{(n)}(\chi_Q; \bar{k})$ are actually *increasing* with m. However, the

$m!$ factor present in the denominator more than compensates for these increasing coefficients and allows us to truncate the series in an actual calculation.

Finally, it is worth pointing out that the case without cutoff on the long-wavelength mode is recovered from the above expression simply by setting $k_l = 0$ and then noting that in this case $\bar{k} = 0$ and that therefore the corresponding terms appearing in Equations (A29) and (A37) disappear.

REFERENCES

Abramowitz, M., & Stegun, I. A. 1965, Handbook of Mathematical Functions: With Formulas, Graphs, and Mathematical Tables (New York: Dover)
Bernardeau, F. 1996, A&A, 312, 11
Bi, H., & Davidsen, A. F. 1997, ApJ, 479, 523
Brandbyge, J., Hannestad, S., Haugboelle, T., & Thomsen, B. 2008, J. Cosmol. Astropart. Phys., JCAP08(2008)020
Croft, R. A. C. 2004, ApJ, 610, 642
Croft, R. A. C., Banday, A. J., & Hernquist, L. 2006, MNRAS, 369, 1090
Croft, R. A. C., Weinberg, D. H., Katz, N., & Hernquist, L. 1998, ApJ, 495, 44
Croft, R. A. C., et al. 2002, ApJ, 581, 20
Eisenstein, D. J., & Hu, W. 1998, ApJ, 496, 605
Fang, T.-T., & White, M. J. 2004, ApJ, 606, L9
Giannantonio, T., Scranton, R., Crittenden, R. G., Nichol, R. C., Boughn, S. P., Myers, A. D., & Richards, G. T. 2008, Phys. Rev. D, 77, 123520
Gnedin, N. Y., & Hui, L. 1998, MNRAS, 296, 44
Gunn, J. E., & Peterson, B. A. 1965, ApJ, 142, 1633
Hincks, A. D., et al. 2010, ApJS, 191, 423
Hirata, C. M., Ho, S., Padmanabhan, N., Seljak, U., & Bahcall, N. A. 2008, Phys. Rev. D, 78, 043520
Hirata, C. M., & Seljak, U. 2003, Phys. Rev. D, 68, 083002
Hui, L., & Gnedin, N. Y. 1997, MNRAS, 292, 27
Hu, W., & Eisenstein, D. J. 1998, ApJ, 498, 497
Hu, W., & Okamoto, T. 2002, ApJ, 574, 566
Kim, T.-S., Bolton, J. S., Viel, M., Haehnelt, M. G., & Carswell, R. F. 2007, MNRAS, 382, 1657
Komatsu, E., et al. 2009, ApJS, 180, 330
Lesgourgues, J., & Pastor, S. 2006, Phys. Rep., 429, 307
Lewis, A., & Challinor, A. 2006, Phys. Rep., 429, 1
Linder, E. V. 2006, Astropart. Phys., 26, 16
McDonald, P. 2003, ApJ, 585, 34
McDonald, P., & Eisenstein, D. J. 2007, Phys. Rev. D, 76, 063009
McDonald, P., et al. 2005, ApJ, 635, 761
McQuinn, M., et al. 2009, ApJ, 694, 842
Peiris, H. V., & Spergel, D. N. 2000, ApJ, 540, 605
Planck Collaboration 2006, The Scientific Programme of *Planck* (Noordwijk: ESA), http://www.rssd.esa.int/index.php?project=Planck
Saitta, F., D'Odorico, V., Bruscoli, M., Cristiani, S., Monaco, P., & Viel, M. 2008, MNRAS, 385, 519
Schlegel, D., White, M., & Eisenstein, D. 2009a, arXiv:0902.4680
Schlegel, D. J., et al. 2009b, arXiv:0904.0468
Scoccimarro, R., & Couchman, H. M. P. 2001, MNRAS, 325, 1312
Seljak, U., McDonald, P., & Makarov, A. 2003, MNRAS, 342, L79
Seljak, U., et al. 2005, Phys. Rev. D, 71, 103515
Slosar, A., Ho, S., White, M., & Louis, T. 2009, J. Cosmol. Astropart. Phys., JCAP10(2009)019
Springel, V. 2005, MNRAS, 364, 1105
Staniszewski, Z., et al. 2009, ApJ, 701, 32
Vallinotto, A., Das, S., Spergel, D. N., & Viel, M. 2009, Phys. Rev. Lett., 103, 091304
Viel, M., Haehnelt, M. G., & Springel, V. 2006, MNRAS, 367, 1655
Viel, M., Haehnelt, M. G., & Springel, V. 2010, J. Cosmol. Astropart. Phys., JCAP06(2010)015
Viel, M., Matarrese, S., Mo, H. J., Haehnelt, M. G., & Theuns, T. 2002, MNRAS, 329, 848
Viel, M., et al. 2004, MNRAS, 347, L26
Xia, J.-Q., & Viel, M. 2009, J. Cosmol. Astropart. Phys., JCAP04(2009)002
Xia, J.-Q., Viel, M., Baccigalupi, C., & Matarrese, S. 2009, J. Cosmol. Astropart. Phys., JCAP09(2009)003
Yoo, J., & Zaldarriaga, M. 2008, Phys. Rev. D, 78, 083002
Zaldarriaga, M., Seljak, U., & Hui, L. 2001, ApJ, 551, 48
Zaroubi, S., Viel, M., Nusser, A., Haehnelt, M., & Kim, T. S. 2006, MNRAS, 369, 734